Fig. 4. *Quantitative analysis of MKK6 and MEK1 expression in the rat aortas. Bars indicate SEM.* $*p < 0.05$ vs. *the WKY group;* $^{\dagger}p < 0.01$ vs. *the vehicle SHRSP group;* $^{\ddagger}p < 0.05$ vs. *the amlodipine group. Experiments:* $n = 6$.
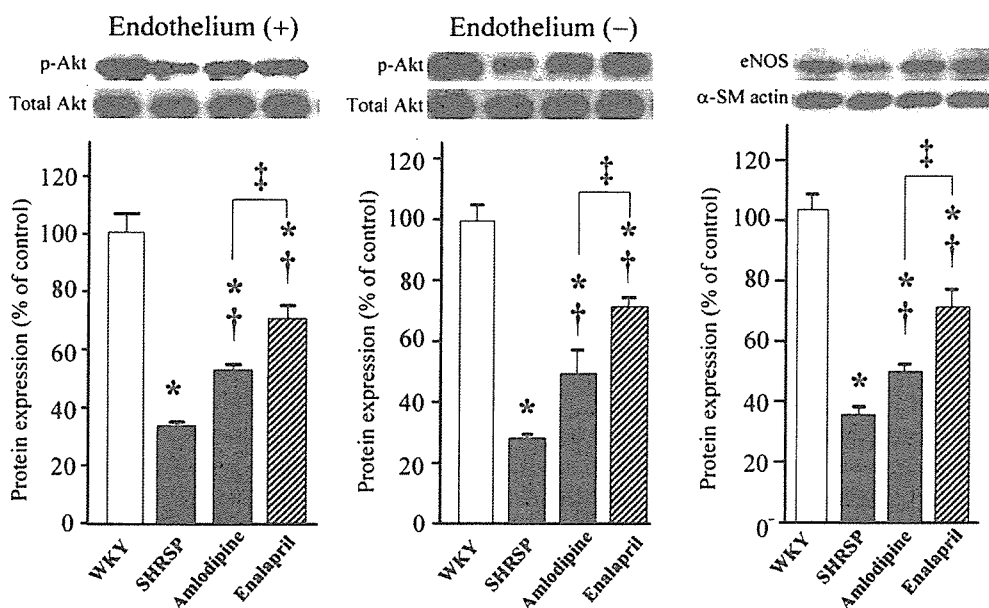

Fig. 5. *Quantitative analysis of p-Akt expression with and without endothelium, and eNOS expression in the rat aortas. Bars indicate SEM.* $*p < 0.01$ vs. *the WKY group;* $^{\dagger}p < 0.05$ vs. *the vehicle SHRSP group;* $^{\ddagger}p < 0.01$ vs. *the amlodipine group. Experiments:* $n = 3-6$.

group. The level of MKK6 and MEK1 expressions in the enalapril group was still significantly greater than that in the WKY group.

Figure 5 shows the results of p-Akt expression in the rat aorta with and without endothelium, and demonstrates that p-Akt was significantly decreased in the vehicle SHRSP group compared with the WKY group. The 2 drug-treated groups had significantly higher p-Akt expression than the vehicle SHRSP group, both with and without endothelium. Enalapril was more effective than amlodipine at increasing p-Akt expression in SHRSP aortas both with and without endothelium.

To clarify whether endothelial dysfunction affects the regulation of the vascular SMC phenotype, we examined the

level of eNOS expression in the rat aortas, and found that the level of eNOS expression was significantly decreased in the vehicle SHRSP group compared with the WKY group (Fig. 5). The two drugs significantly restored eNOS expressions in SHRSP aortas, but the levels of eNOS expression in the 2 drug-treated groups were still lower than that in the WKY group. Enalapril was more effective than amlodipine at restoring eNOS expression in SHRSP aortas.

Discussion

In this study, we demonstrated that within 6 weeks and at the doses used, both amlodipine and enalapril significantly and equally reduced blood pressure, and shifted vascular SMCs in the SHRSP aorta toward the differentiated (contractile) type by reducing NMHC-B/SMemb and increasing SM2, and inducing equipotent inhibition of the MKK6 and p38 MAPK pathways. The major differences in the effects of amlodipine and enalapril on signaling pathways for aortic SMC differentiation in SHRSP observed in our experiments were as follows: amlodipine induced a significantly greater reduction in MEK1 and p-42/44 ERK compared with enalapril, whereas enalapril was more effective than amlodipine at increasing p-Akt and eNOS in SHRSP aortas.

Meta-analyses of the recent clinical trials in hypertension suggest that blood pressure control is important, and that all antihypertensive drugs, including calcium antagonists and ACE inhibitors, have similar long-term efficacy and safety (6–8). In addition, it has been demonstrated that amlodipine improved left ventricular hypertrophy by controlling 24-h blood pressure (14), and reduced the rate of atherosclerosis in the carotid arteries as assessed by B-mode ultrasonography with fewer cases of cardiac events compared to the placebo in patients with coronary artery disease (11). Furthermore, in a study that measured the progression of atherosclerosis using intravascular ultrasound, administration of amlodipine but not enalapril reduced adverse cardiovascular events and retarded atherosclerosis progression in patients with coronary artery disease and normal blood pressure (12). These results suggest that amlodipine, as a vascular protective agent, may effectively improve outcomes in high-risk patients with coronary artery disease (15). However, the precise mechanism of the antiatherogenic property of amlodipine in hypertension has remained obscure.

Since the main function of vascular SMCs is Ca^{2+}-dependent contraction controlled by actin-myosin linked dual regulation (16, 17), dihydropyridine calcium antagonists play an important role in the treatment of hypertension by lowering blood pressure through a mechanism of blocking L-type calcium channels in vascular SMCs, which express a large number of voltage-dependent calcium channels (18). In addition, several potential antiatherosclerotic mechanisms of pleiotropic action independent of L-type calcium channel modulation have been reported for amlodipine (10–12, 15), including inhibition of lipid peroxide formation, increase in NO produc-

tion, modification of SMC atherosclerotic membrane defects, a proteoglycan-mediated mechanism by vascular SMCs and low-density lipoprotein–proteoglycan interaction, and SMC phenotypic change, proliferation, and migration through potent inhibition of Ca^{2+} movements involved in cell-cycle initiation/progression (19, 20). These cellular actions by amlodipine would inhibit vascular remodeling (10, 15). We recently reported that both enalapril and amlodipine might have additional benefits for the reduction of oxidative stress, vascular remodeling, and cardiac fibrosis in SHRSP hearts beyond blood-pressure lowering, and that amlodipine inhibited vascular remodeling of intramyocardial arteries in SHRSP by efficiently modifying Cu/Zn superoxide dismutase, more so than did enalapril (13). Amlodipine may also have antioxidant properties in addition to antihypertensive activity to inhibit neuronal cell death (21), which would be useful to prevent cerebrovascular accidents in hypertensive patients. It has also been reported that amlodipine exerts its potent growth inhibitory effects by inhibiting the expression of early growth–response genes (10–12, 22–24), and by interfering with multiple branches of mitogenic signaling pathways (19, 25–27). Furthermore, Stepien et al. also reported that amlodipine specifically alters Ca^{2+} mobilization by interacting with the sarcoplasmic reticulum and inhibiting voltage-dependent Ca^{2+} influx and the resulting ERK activation (22).

The phenotypic modulation of vascular SMCs is a hallmark of vascular dysfunction in hypertension (1, 2). However, the mechanisms regulating vascular SMC phenotypic modulation and the critical signal transductions affecting the vascular SMC phenotype remain controversial (3, 28–31). Under culture conditions that maintained cultured vascular SMCs in the differentiated type, which is similar to the *in vivo* phenotype, Hayashi et al. recently demonstrated that maintenance of a differentiated phenotype of SMCs depends on the Akt pathway, whereas the coordinate activation of the ERK and p38 MAPK pathways induces SMC de-differentiation (5), indicating that the SMC phenotype should be determined by the balance between the strengths of the Akt pathway and the ERK and p38 MAPK pathways. We also reported that the ACE inhibitor cilazapril might inhibit NAD(P)H oxidase activity and shifted vascular SMCs in the SHRSP aorta toward the differentiated (contractile) type, and that the Akt pathway, but not the p38 MAPK or ERK pathways, may play a key role in determining SMC differentiation in the SHRSP aorta *in vivo* (3). Our results for enalapril in the present experiments are consistent with those of our previous reports (3), suggesting that enalapril may induce differentiation (contractility) of SMCs in SHRSP aortas, and that the balance and cross-regulation between the Akt- and MEK-signaling cascades determine the temporal pattern of ERK phosphorylation and may thereby guide the phenotypic modulation of vascular SMCs (32). Furthermore, we showed that both amlodipine and enalapril increased Akt in SHRSP aortas with or without an endothelium, suggesting that the Akt present not

only in the endothelium but also in the media may participate in the regulation of SMC phenotypic change in SHRSP aortas. Since the blood pressure–lowering actions of amlodipine and enalapril were equal, and no significant differences were observed in the reduction of the expressions of p38 MAPK and ERK between the 2 drug-treated groups, the activations of the p38 MAPK and ERK cascades in SHRSP aortas might be mainly dependent on blood pressure rather than on the drugs used.

Hypertension is a central pathogenic factor of endothelial dysfunction that is caused, in part, by the impairment of endothelial NO production by eNOS (*3*, *33*). Dihydropyridine calcium antagonists also modulate endothelial functions by "pleiotropic effects" such as enhancement of the bioavailability of endothelial NO, which plays a pivotal role in the regulation of vasorelaxation, leukocyte adhesion and platelet aggregation; impaired NO release is associated with the genesis and progression of atherosclerotic diseases and an increase in endothelial NO formation (*10*), which may contribute to the antiatherogenic effects of amlodipine (*34*). ACE inhibitors also attenuate endothelial dysfunction and enhance NO release from the vascular endothelium, which may contribute to the reduction of vascular structural alterations (*35*). Furthermore, On *et al*. demonstrated that treatment with an ACE inhibitor or a calcium antagonist resulted in improvement by a mechanism that is probably related to antioxidant activity (*33*). Our findings in the endothelium are consistent with those of our previous reports (*3*, *13*), suggesting that both types of drugs may restore the level of NO by increasing eNOS to induce differentiation of vascular SMCs.

Furthermore, within 6 weeks and at the doses used, enalapril may have restored eNOS by inducing a greater change than amlodipine in SHRSP aortas in our experimental model. Although the MEK-ERK pathway present in the endothelium may be involved in the effects of amlodipine on SMC phenotypic change in SHRSP aortas, based upon our findings the MEK-ERK pathway present in vascular SMCs may be more important for the phenotypic change of vascular SMCs compared with that present in the endothelium: amlodipine significantly reduced the MEK1 and p-42/44 ERK expression, while there was a significant difference in their expression in SHRSP aortas between the amlodipine and enalapril groups, even though the eNOS expression could not be restored to the same level as that of the WKY group by the administration of either drug. It has also been reported that inhibition of MEK1/2 does not alter blood pressure despite improved endothelial function and reduced arterial reactivity to Ang II (*36*), which may support our conclusions.

There are several limitations present in this study. We cannot exclude the possibility that signal transductions other than the MEK-ERK pathway may have been involved in the SMC phenotypic change in the aorta induced by the calcium antagonist amlodipine, since it has been reported that a variety of factors—such as hemodynamic and mechanical forces, and biochemical, cytokine and extracellular matrix stimulation—

could lead to changes in SMC phenotype (*37*, *38*). In our study, blood pressures in SHRSP treated for 6 weeks with amlodipine at the doses used were still significantly higher compared with those in WKY, and p-42/44 ERK expression in the SHRSP aorta was significantly higher than that in the WKY while MEK1, the upstream kinase of ERK, decreased to the same level as in the WKY. It is likely that the 6-week treatment of SHRSP with amlodipine was not long enough to decrease aortic p-42/44 ERK expression to the level seen in the WKY in our experiments.

In summary, our study demonstrated that enalapril and amlodipine inhibited SMC de-differentiation through the inhibition of the MEK1-ERK pathway as well as the MKK6-p38 MAPK pathway, and through the upregulation of the eNOS and Akt pathways in SHRSP aortas. Furthermore, amlodipine was more effective than enalapril at reducing the MEK-ERK pathway and increasing SM2 expression in SHRSP aortas at the doses used, suggesting that the MEK-ERK pathways might be one of the crucial determinants for the phenotypic change of vascular SMCs, which in turn might be responsible for the antiatherogenic property of amlodipine in hypertension *in vivo*. Further studies will be required to understand the detailed signaling pathways that regulate the vascular SMC phenotype and the functional linkage between such signaling pathways *in vivo*.

References

1. Owens GK: Regulation of differentiation of vascular smooth muscle cells. *Physiol Rev* 1995; **75**: 487–517.
2. Fujii K, Umemoto S, Fujii A, *et al*: Angiotensin II type 1 receptor antagonist downregulates nonmuscle myosin heavy chains in spontaneously hypertensive rat aorta. *Hypertension* 1999; **33**: 975–980.
3. Kawahara S, Umemoto S, Tanaka M, *et al*: Up-regulation of Akt and eNOS induces vascular smooth muscle cell differentiation in hypertension *in vivo*. *J Cardiovasc Pharmacol* 2005; **45**: 367–374.
4. Kubo M, Umemoto S, Fujii K, *et al*: Effects of angiotensin II type 1 receptor antagonist on smooth muscle cell phenotype in intramyocardial arteries from spontaneously hypertensive rats. *Hypertens Res* 2004; **27**: 685–693.
5. Hayashi K, Takahashi M, Kimura K, *et al*: Changes in the balance of phosphoinositide 3-kinase/protein kinase B (Akt) and the mitogen-activated protein kinases (ERK/p38MAPK) determine a phenotype of visceral and vascular smooth muscle cells. *J Cell Biol* 1999; **145**: 727–740.
6. Opie LH, Schall R: Evidence-based evaluation of calcium channel blockers for hypertension: equality of mortality and cardiovascular risk relative to conventional therapy. *J Am Coll Cardiol* 2002; **39**: 315–322.
7. Staessen JA, Wang JG, Thijs L: Cardiovascular protection and blood pressure reduction: a meta-analysis. *Lancet* 2001;

358: 1305–1315.

8. Staessen JA, Li Y, Thijs L, *et al*: Blood pressure reduction and cardiovascular prevention: an update including the 2003–2004 secondary prevention trials. *Hypertens Res* 2005; **28**: 385–407.

9. ALLHAT Officers and Coordinators for the ALLHAT Collaborative Research Group: Major outcomes in high-risk hypertensive patients randomized to angiotensin-converting enzyme inhibitor or calcium channel blocker *vs* diuretic: the Antihypertensive and Lipid-Lowering Treatment to Prevent Heart Attack Trial (ALLHAT). *JAMA* 2002; **288**: 2981–2997.

10. Mason RP, Marche P, Hintze TH: Novel vascular biology of third-generation L-type calcium channel antagonists: ancillary actions of amlodipine. *Arterioscler Thromb Vasc Biol* 2003; **23**: 2155–2163.

11. Pitt B, Byington RP, Furberg CD, *et al*, for the PREVENT Investigators: Effect of amlodipine on the progression of atherosclerosis and the occurrence of clinical events. *Circulation* 2000; **102**: 1503–1510.

12. Nissen SE, Tuzcu EM, Libby P, *et al*: Effect of antihypertensive agents on cardiovascular events in patients with coronary disease and normal blood pressure: the CAMELOT study: a randomized controlled trial. *JAMA* 2004; **292**: 2217–2225.

13. Umemoto S, Tanaka M, Kawahara S, *et al*: Calcium antagonist reduces oxidative stress by upregulating Cu/Zn superoxide dismutase in stroke-prone spontaneously hypertensive rats. *Hypertens Res* 2004; **27**: 877–885.

14. Ishimitsu T, Kobayashi T, Honda T, *et al*: Protective effects of an angiotensin II receptor blocker and a long-acting calcium channel blocker against cardiovascular organ injuries in hypertensive patients. *Hypertens Res* 2005; **28**: 351–359.

15. Mason RP: Mechanisms of plaque stabilization for the dihydropyridine calcium channel blocker amlodipine: review of the evidence. *Atherosclerosis* 2002; **165**: 191–199.

16. Umemoto S, Sellers JR: Characterization of *in vitro* motility assays using smooth muscle and cytoplasmic myosins. *J Biol Chem* 1990; **265**: 14864–14869.

17. Sobue K, Hayashi K, Nishida W: Molecular mechanism of phenotypic modulation of smooth muscle cells. *Horm Res* 1998; **50** (Suppl 2): 15–24.

18. Gollasch M, Haase H, Ried C, *et al*: L-type calcium channel expression depends on the differentiated state of vascular smooth muscle cells. *FASEB J* 1998; **12**: 593–601.

19. Stepien O, Zhang Y, Zhu D, *et al*: Dual mechanism of action of amlodipine in human vascular smooth muscle cells. *J Hypertens* 2002; **20**: 95–102.

20. Berridge MJ: Unlocking the secrets of cell signaling. *Annu Rev Physiol* 2005; **67**: 1–21.

21. Yamagata K, Ichinose S, Tagami M: Amlodipine and carvedilol prevent cytotoxicity in cortical neurons isolated from stroke-prone spontaneously hypertensive rats. *Hypertens Res* 2004; **27**: 271–282.

22. Stepien O, Gogusev J, Zhu DL, *et al*: Amlodipine inhibition of serum-, thrombin-, or fibroblast growth factor–induced vascular smooth-muscle cell proliferation. *J Cardiovasc Pharmacol* 1998; **31**: 786–793.

23. Ko Y, Totzke G, Graack GH, *et al*: Action of dihydropyridine calcium antagonists on early growth response gene

expression and cell growth in vascular smooth muscle cells. *J Hypertens* 1993; **11**: 1171–1178.

24. Mancini GB: Antiatherosclerotic effects of calcium channel blockers. *Prog Cardiovasc Dis* 2002; **45**: 1–20.

25. Zhang YZ, Gao PJ, Wang XY, *et al*: The inhibitory mechanisms of amlodipine in human vascular smooth muscle cell proliferation. *Hypertens Res* 2000; **23**: 403–406.

26. Lai YM, Fukuda N, Su JZ, *et al*: Novel mechanisms of the antiproliferative effects of amlodipine in vascular smooth muscle cells from spontaneously hypertensive rats. *Hypertens Res* 2002; **25**: 109–115.

27. Jackson CL, Bush RC, Bowyer DE: Mechanism of antiatherogenic action of calcium antagonists. *Atherosclerosis* 1989; **80**: 17–26.

28. Laplante MA, Wu R, El Midaoui A, *et al*: NAD(P)H oxidase activation by angiotensin II is dependent on p42/44 ERK-MAPK pathway activation in rat's vascular smooth muscle cells. *J Hypertens* 2003; **21**: 927–936.

29. Touyz RM, El Mabrouk M, He G, *et al*: Mitogen-activated protein/extracellular signal–regulated kinase inhibition attenuates angiotensin II–mediated signaling and contraction in spontaneously hypertensive rat vascular smooth muscle cells. *Circ Res* 1999; **84**: 505–515.

30. Su B, Mitra S, Gregg H, *et al*: Redox regulation of vascular smooth muscle cell differentiation. *Circ Res* 2001; **89**: 39–46.

31. Ushio-Fukai M, Alexander RW, Akers M, *et al*: Reactive oxygen species mediate the activation of Akt/protein kinase B by angiotensin II in vascular smooth muscle cells. *J Biol Chem* 1999; **274**: 22699–22704.

32. Reusch HP, Zimmermann S, Schaefer M, *et al*: Regulation of Raf by Akt controls growth and differentiation in vascular smooth muscle cells. *J Biol Chem* 2001; **276**: 33630–33637.

33. On YK, Kim CH, Oh BH, *et al*: Effects of angiotensin converting enzyme inhibitor and calcium antagonist on endothelial function in patients with essential hypertension. *Hypertens Res* 2002; **25**: 365–371.

34. Berkels R, Taubert D, Rosenkranz A, *et al*: Vascular protective effects of dihydropyridine calcium antagonists. Involvement of endothelial nitric oxide. *Pharmacology* 2003; **69**: 171–176.

35. Gohlke P, Stoll M, Lamberty V, *et al*: Cardiac and vascular effects of chronic angiotensin converting enzyme inhibition at subantihypertensive doses. *J Hypertens Suppl* 1992; **10**: S141–S144.

36. Touyz RM, Deschepper C, Park JB, *et al*: Inhibition of mitogen-activated protein/extracellular signal–regulated kinase improves endothelial function and attenuates Ang II–induced contractility of mesenteric resistance arteries from spontaneously hypertensive rats. *J Hypertens* 2002; **20**: 1127–1134.

37. Stegemann JP, Hong H, Nerem RM: Mechanical, biochemical, and extracellular matrix effects on vascular smooth muscle cell phenotype. *J Appl Physiol* 2005; **98**: 2321–2327.

38. Raines EW, Ferri N: Thematic review series: the immune system and atherogenesis. Cytokines affecting endothelial and smooth muscle cells in vascular disease. *J Lipid Res* 2005; **46**: 1081–1092.

Usefulness of Mitral Annular Velocity in Predicting Exercise Tolerance in Patients With Impaired Left Ventricular Systolic Function

Yasuyuki Hadano, MD[a,*], Kazuya Murata, MD[a], Takeshi Yamamoto, MD[a],
Hideki Kunichika, MD[a], Tomo Matsumoto, MD[a], Eizo Akagawa, MD[a], Takashi Sato, MD[a],
Takeo Tanaka, MD[a], Yoshio Nose, MD[a], Nobuaki Tanaka, MD[b],
and Masunori Matsuzaki, MD[a]

Left ventricular (LV) diastolic function is 1 of the determinants of exercise tolerance. However, the relation between early diastolic velocity of the mitral annulus (Ea) obtained by tissue Doppler imaging and exercise tolerance is unknown in patients with impaired LV systolic function. To investigate the feasibility of evaluating exercise tolerance using tissue Doppler imaging, we studied 53 consecutive patients (mean age 58 ± 14 years) with a LV ejection fraction of <50% (mean 37 ± 9%). We measured the peak early diastolic velocity of transmitral flow (E) and Ea at the lateral border of the mitral annulus and then calculated the E/Ea ratio. After echocardiography, we measured the peak oxygen consumption and anaerobic threshold (AT) by cardiopulmonary exercise testing. Of all the echocardiographic parameters, the best correlation for AT was the E/Ea ratio ($r = -0.74$, $p < 0.001$). Peak oxygen consumption correlated well with Ea and the E/Ea ratio ($r = 0.64$ and $r = -0.68$, respectively, $p < 0.001$). The AT and peak oxygen consumption did not correlate with conventional Doppler indexes. Using an AT of 8 ml/min/kg as the cutoff to separate severe exercise intolerance from normal, mild, or moderate exercise intolerance, a receiver-operating characteristic curve showed that an E/Ea ratio of >11.3 had the best combination of sensitivity (88%) and specificity (86%). Exercise tolerance correlated with the E/Ea ratio in patients with impaired LV systolic function. In conclusion, the evaluation of LV diastolic function using tissue Doppler imaging is useful for predicting exercise tolerance in patients with heart failure. © 2006 Elsevier Inc. All rights reserved. (Am J Cardiol 2006;97:1025–1028)

Tissue Doppler imaging (TDI) has enabled us to acquire myocardial velocities online during ultrasound examinations. The early diastolic velocity of the mitral annulus (Ea) measured using TDI has been reported to be a preload independent index for evaluating left ventricular (LV) diastolic function.[1,2] In this study, we sought to determine the relation between early diastolic mitral annular velocities combined with conventional Doppler indexes and exercise tolerance in patients with impaired LV systolic function and the usefulness of mitral annular velocities in the prediction of exercise tolerance in these patients.

Methods

Study population: We studied 53 consecutive patients (36 men and 17 women; mean age 58 ± 14 years) with impaired LV systolic function who had been referred for cardiopulmonary exercise testing. All patients were in sinus rhythm and had a normal PQ interval on an electrocardiogram and a LV ejection fraction of <50% without moderate or severe mitral regurgitation. The range of LV ejection fraction was 18% to 49% (mean 37 ± 9%). Patients with evidence of ischemia during the stress test, atrial fibrillation, or chronic obstructive pulmonary disease were excluded. The clinical and echocardiographic characteristics are listed in Table 1. The institutional review boards of Yamaguchi University Hospital approved the investigational protocol, and all patients gave written informed consent before participation.

Echocardiography: All patients were examined by transthoracic echocardiography before starting cardiopulmonary exercise testing. The echocardiographic measurements were performed in a blinded manner. The examinations were performed with patients in the left lateral position. An ultrasound instrument with a 2.5-MHz transducer (System Five or Vivid Seven, Vingmed, Horten, Norway) was used. All data were recorded during end-expiratory apnea. The LV ejection fraction was calculated using a biplane method of disks.

All Doppler profiles were recorded as previously described.[3] The peak velocities of early (E) and late (A) mitral

Table 1
Patient characteristics (n = 53)

Variable	
Age (yrs)	58 ± 14
Men/women	36/17
Height (cm)	161 ± 9
Weight (kg)	60 ± 14
Body mass index (kg/m^2)	23.0 ± 4.0
LV ejection fraction (%)	37 ± 9
LV end-diastolic dimension (mm)	60 ± 8
LV end-systolic dimension (mm)	47 ± 9
LV septal thickness (mm)	9.7 ± 2.6
LV posterior thickness (mm)	9.9 ± 1.7
Left atrial dimension (mm)	40 ± 7
Congestive heart failure (history)	28 (53%)
New York Heart Association class	
I	9 (17%)
II	35 (66%)
III	9 (17%)
Clinical diagnosis	
Dilated cardiomyopathy	19 (36%)
Healed myocardial infarction	15 (28%)
Aortic valvular disease	7 (13%)
Hypertrophic cardiomyopathy (dilated phase)	3 (6%)
Hypertensive heart disease	3 (6%)
Other	6 (11%)

Data are presented as means ± SDs or numbers (percentages).

Table 2
Correlation coefficients of echocardiographic indexes with anaerobic threshold (AT) or peak oxygen consumption (P$\dot{V}O_2$)

Variable	AT		P$\dot{V}O_2$	
	r	p	r	p
E	−0.15	0.28	0.12	0.40
A	−0.16	0.24	−0.22	0.12
E/A	−0.11	0.44	0.07	0.65
DcT	0.14	0.33	0.11	0.46
MAd	0.31	<0.05	0.36	<0.01
Vp	0.41	<0.01	0.48	<0.001
E/Vp	−0.57	<0.001	−0.37	<0.01
Sa	0.35	<0.05	0.36	<0.05
Ea	0.43	<0.01	0.64	<0.001
E/Ea	−0.74	<0.001	−0.68	<0.001
Aa	0.08	0.58	0.12	0.41
Ea/Aa	0.29	<0.05	0.47	<0.001
LV ejection fraction	0.44	<0.001	0.43	<0.01
LV end-diastolic dimension	−0.04	0.80	0.03	0.83
Left atrial dimension	−0.22	0.12	−0.21	0.14

DcT = deceleration time of the early diastolic wave of transmitral flow; MAd = mitral A duration.

inflow, deceleration time of the E wave, and mitral A duration were measured using pulse-wave Doppler with the sample volume at the tip of mitral valve leaflets. We also measured the color M-mode Doppler flow propagation velocity of LV inflow (Vp) as the slope of the first aliasing velocity (45 cm/s) during early filling, from the mitral valve plane to 4 cm distally into the LV cavity. TDI of the mitral annulus was obtained from an apical 4-chamber view, using a 1- to 2-mm sample volume placed in the lateral mitral annulus. The peak systolic, early (Ea), and late (Aa) diastolic velocities were measured from the TDI recordings. The E/A, E/Vp, E/Ea, and Ea/Aa ratios were calculated. In each patient, the velocity waves of 3 consecutive cardiac cycles obtained during end-expiratory apnea were averaged.

Cardiopulmonary exercise testing: After the echocardiographic examinations, all patients underwent symptom-limited exercise tests on an upright bicycle ergometer using a ramp protocol with simultaneous respiratory gas analysis and blood pressure recording. A physician who was unaware of the echocardiographic results was present during all the studies to encourage maximal exertion. Expired oxygen, carbon dioxide, and airflow rate were measured continuously at rest and throughout exercise using a breathing apparatus. The peak oxygen consumption (P$\dot{V}O_2$), defined as the mean of the highest oxygen consumption values obtained during the last 10 seconds of exercise, and the anaerobic threshold (AT), defined as the point at which carbon dioxide production increased disproportionately in relation to oxygen consumption obtained from a graph plot-

ting oxygen consumption against carbon dioxide production, were measured.

Statistical analysis: The results are expressed as means ± SDs. Statistical analysis was performed using a statistical package (Stat-view, Berkeley, California). Pearson's correlation was used to evaluate the correlations of Doppler echocardiographic parameters with the P$\dot{V}O_2$ and AT. A p level of <0.05 was considered significant. A receiver-operating characteristic curve was plotted to determine the sensitivity and specificity of the different E/Ea values to predict severe exercise intolerance at an AT of <8 ml/min/kg.[4]

Results

The clinical characteristics and echocardiographic data are listed in Table 1. Of 53 patients, 28 (53%) had a history of congestive heart failure and 44 (83%) had exertional dyspnea (New York Heart Association functional class II [n = 35] and III [n = 9]). Of the 53 patients, 16 (30%) achieved an AT of <8 ml/min/kg. The correlations between the echocardiographic parameters and AT or P$\dot{V}O_2$ are presented in Table 2.

A significant positive correlation was found between the P$\dot{V}O_2$ and Ea (r = 0.64, p <0.001). The AT and P$\dot{V}O_2$ correlated well with the E/Ea ratio (r = −0.74 and r = −0.68, respectively, p <0.001). Of all the echocardiographic parameters measured, the best correlation for AT was the E/Ea ratio. The AT correlated weakly or modestly with Vp, the E/Vp ratio, and LV ejection fraction and did not correlate with the conventional Doppler indexes, LV size, or left atrial size.

Using an AT of 8 ml/min/kg as the cutoff to separate

severe exercise intolerance from normal, mild, or moderate exercise intolerance,[4] a receiver-operating characteristic curve showed that an E/Ea ratio of >11.3 had the best combination of sensitivity (88%) and specificity (86%). The area under the receiver-operating characteristic curve using the E/Ea ratio to predict an AT of <8 ml/min/kg was 0.91.

Discussion

In the present study, we showed that, unlike LV ejection fraction or conventional Doppler indexes alone, the E/Ea ratio correlated well with exercise tolerance in patients with impaired LV systolic function. To our knowledge, this is the first study to identify the determinants of exercise tolerance using TDI in patients with impaired LV systolic function.

Although many studies have reported the relation between echocardiographic indexes and exercise tolerance,[5-8] their subjects were limited to those with preserved LV systolic function. Exercise tolerance is an important factor for managing patients with impaired LV systolic function or heart failure. Therefore, we focused on patients with impaired LV systolic function in this study.

Conventional Doppler indexes, such as peak A velocity or E/A, have been shown to be important contributors to exercise tolerance in normal patients and patients with various heart diseases.[5,9] In our study, conventional diastolic Doppler indexes showed no correlations with exercise tolerance, similar to the findings of previous reports.[6-8]

Mitral E-wave velocity is influenced by multiple interrelated factors, including LV relaxation rate, atrial and ventricular compliance, and left atrial pressure.[10] In diseased ventricles, progressive shortening of the transmitral deceleration time of the E wave and increasing E/A ratios can be seen with decreasing ventricular compliance and increasing LV filling pressures.[11,12] To overcome these limitations in mitral inflow parameters, combinations of mitral flow velocity curves with other Doppler parameters have been proposed. TDI is a recently developed echocardiographic modality used to measure tissue velocity focusing on lower velocity frequency shifts. Mitral annular motion obtained by TDI has been introduced to correct for the influences of preload and myocardial relaxation on transmitral flow and has been shown to be an excellent predictor of diastolic filling in subsets of patients.[2,13-15]

Previous studies have shown that elevated LV filling pressures may cause exertional dyspnea and exercise intolerance in patients with heart failure.[16,17] Recently, it has been shown that LV filling pressures correlated with the E/Ea ratio.[2,13-15] Our results have also suggested that elevated LV filling pressures, as determined by the E/Ea ratio, was the strongest predictor of reduced exercise tolerance. Most published studies have shown relatively weak or inconsistent relations between the mitral flow profile alone and exercise tolerance[6,8] or LV filling pressures.[2,13-15] The poor correlations occurred because transmitral flow veloci-

ties are influenced not only by LV relaxation rate but also by preload, heart rate, age, and LV compliance.[10] Conversely, several groups have shown excellent correlations between the E/Ea ratio and LV filling pressures.[2,13-15]

Similar to previous investigators,[6-8] we found that conventional Doppler indexes and Vp were weak predictors of exercise performance. Vp is an index of LV relaxation and correlates inversely with the time constant of LV isovolumetric relaxation,[18] and the E/Vp ratio correlates with LV filling pressures.[19] In our study, Vp and the E/Vp ratio correlated with exercise tolerance; however, the correlations were weak or modest compared with the E/Ea ratio. In contrast to the Vp, Ea is easily recorded and measured with TDI and is independent of LV systolic function; Vp is currently measured by varying methods and appears to have some relation to systolic performance.[18,19] Thus, the E/Ea ratio, which is relatively simple to obtain, conceptually has the potential for providing a reasonable estimate of exercise tolerance throughout a wide range of relaxation abnormalities.

This study had several limitations. First, because LV diastolic filling and exercise tolerance can be influenced by various parameters, including age, heart rate, loading conditions, and the patient's position, it is possible that some unaccounted factors influencing these 2 parameters contributed to our results. Finally, other factors, such as a reduced stroke volume response, ventilation/perfusion mismatch, and abnormal peripheral oxygen use also influence exercise limitation. Additional studies are needed to determine the exact mechanisms of exercise intolerance.

1. Sohn D-W, Chai I-H, Lee D-J, Kim H-C, Kim H-S, Oh B-H, Lee M-M, Park Y-B, Choi Y-S, Seo J-D, Lee Y-W. Assessment of mitral annulus velocity by Doppler tissue imaging in the evaluation of left ventricular diastolic function. *J Am Coll Cardiol* 1997;30:474–480.
2. Nagueh SF, Middleton KJ, Kopelen HA, Zoghbi WA, Quinones MA. Doppler tissue imaging: a noninvasive technique for evaluation of left ventricular relaxation and estimation of filling pressures. *J Am Coll Cardiol* 1997;30:1527–1533.
3. Hadano Y, Murata K, Liu J, Oyama R, Harada N, Okuda S, Hamada Y, Tanaka N, Matsuzaki M. Can transthoracic Doppler echocardiography predict the discrepancy between left ventricular end-diastolic pressure and mean pulmonary capillary wedge pressure in patients with heart failure? *Circ J* 2005;69:432–438.
4. Weber KT, Janicki JS, McElroy PA. Cardiopulmonary exercise (CPX) testing. In: Weber KT, Janicki JS, eds. Cardiopulmonary Exercise Testing. Philadelphia: WB Saunders, 1986:151–167.
5. Okura H, Inoue H, Tomon M, Nishiyama S, Yoshikawa T, Yoshida K, Yoshikawa J. Impact of Doppler-derived left ventricular diastolic performance on exercise capacity in normal individuals. *Am Heart J* 2000;139:716–722.
6. Matsumura Y, Elliott PM, Virdee MS, Sorajja P, Doi Y, McKenna WJ. Left ventricular diastolic function assessed using Doppler tissue imaging in patients with hypertrophic cardiomyopathy: relation to symptoms and exercise capacity. *Heart* 2002;87:247–251.
7. Kim H-K, Kim Y-J, Cho Y-S, Sohn D-W, Lee M-M, Park Y-B, Choi Y-S. Determinants of exercise capacity in hypertensive patients: new insights from tissue Doppler echocardiography. *Am J Hypertens* 2003; 16:564–569.

8. Skaluba SJ, Litwin SE. Mechanisms of exercise intolerance: insights from tissue Doppler imaging. *Circulation* 2004;109:972–977.

9. Lapu-Bula R, Robert A, de Kock M, D'Hondt A-M, Detry J-M, Melin JA, Vanoverschelde J-L. Relation of exercise capacity to left ventricular systolic function and diastolic filling in idiopathic or ischemic dilated cardiomyopathy. *Am J Cardiol* 1999;83:728–734.

10. Appleton CP, Hatle LK, Popp RL. Relation of transmitral flow velocity patterns to left ventricular diastolic function: new insights from a combined hemodynamic and Doppler echocardiographic study. *J Am Coll Cardiol* 1988;12:426–440.

11. Giannuzzi P, Imparato A, Temporelli PL, de Vito F, Silva PL, Scapellato F, Giordano A. Doppler-derived mitral deceleration time of early filling as a strong predictor of pulmonary capillary wedge pressure in postinfarction patients with left ventricular systolic dysfunction. *J Am Coll Cardiol* 1994;23:1630–1637.

12. Yamamoto K, Nishimura RA, Chaliki HP, Appleton CP, Holmes DR Jr, Redfield MM. Determination of left ventricular filling pressure by Doppler echocardiography in patients with coronary artery disease: critical role of left ventricular systolic function. *J Am Coll Cardiol* 1997;30:1819–1826.

13. Ommen SR, Nishimura RA, Appleton CP, Miller FA, Oh JK, Redfield MM, Tajik AJ. Clinical utility of Doppler echocardiography and tissue Doppler imaging in the estimation of left ventricular filling pressures: a comparative simultaneous Doppler-catheterization study. *Circulation* 2000;102:1788–1794.

14. Rivas-Gotz C, Manolios M, Thohan V, Nagueh SF. Impact of left ventricular ejection fraction on estimation of left ventricular filling pressures using tissue Doppler and flow propagation velocity. *Am J Cardiol* 2003;91:780–784.

15. Dokainish H, Zoghbi WA, Lakkis NM, Al-Bakshy F, Dhir M, Quinones MA, Nagueh SF. Optimal noninvasive assessment of left ventricular filling pressures: a comparison of tissue Doppler echocardiography and B-type natriuretic peptide in patients with pulmonary artery catheters. *Circulation* 2004;109:2432–2439.

16. Szlachcic J, Massie BM, Kramer BL, Topic N, Tubau J. Correlates and prognostic implication of exercise capacity in chronic congestive heart failure. *Am J Cardiol* 1985;55:1037–1042.

17. Kitzman DW, Higginbotham MB, Cobb FR, Sheikh KH, Sullivan MJ. Exercise intolerance in patients with heart failure and preserved left ventricular systolic function: failure of the Frank-Starling mechanism. *J Am Coll Cardiol* 1991;17:1065–1072.

18. Takatsuji H, Mikami T, Urasawa K, Teranishi J, Onozuka H, Takagi C, Makita Y, Matsuo H, Kusuoka H, Kitabatake A. A new approach for evaluation of left ventricular diastolic function: spatial and temporal analysis of left ventricular filling flow propagation by color M-mode Doppler echocardiography. *J Am Coll Cardiol* 1996;27:365–371.

19. Garcia MJ, Ares MA, Asher C, Rodriguez L, Vandervoort P, Thomas JD. An index of early left ventricular filling that combined with pulsed Doppler peak E velocity may estimate capillary wedge pressure. *J Am Coll Cardiol* 1997;29:448–454.

Tricuspid Pouch can Cause Systemic Embolization in Adulthood

Akira Takaki, MD; Hiroshi Ogawa, MD; Takatoshi Wakeyama, MD; Takahiro Iwami, MD;
Masayuki Kimura, MD; Hitoshi Uchinoumi, MD; Shintarou Akashi, MD;
Susumu Matsuda, MD; Yousuke Miyazaki, MD; Masunori Matsuzaki, MD*;
Haruhiko Okada, MD**; Masahiko Nishida, MD**; Masanori Murakami, MD**

A 63-year-old-man with significant left hemiplegia was admitted to hospital. He had experienced a transient cerebral ischemic attack 10 years ago. Computed tomography revealed hypodensity along the right lateral ventricle, which corresponded to the left paralysis. Echocardiography and left ventricular angiography revealed an aneurysm of the membranous septum (AMS) without a ventricular septal defect (VSD). Therefore, the embolism was thought to be of cardiac origin, but surgery revealed that it was not caused by AMS. The aneurysm was created when the septal leaflet of tricupid valve formed a giant capsule during the process of natural closure of the VSD. It was a large pouch, 2.0 cm in diameter, adjacent to the septal leaflet. Anomalies of the tricuspid valve, including pouches, can resemble AMS. (*Circ J* 2006; **70**: 631–633)

Key Words: Aneurysm; Cerebral infarction; Embolism; Membranous septum; Tricuspid pouch

The ricuspid pouch is a pouch-like structure that bulges into the right ventricle near the interventricular membranous septum. It is commonly reported at postmortem examination of infants, but is rarely seen in adults. Hamby et al reported aneurysm of the pars membranacea for the first time in 1970! The septal leaflet of the tricuspid valve formed an irregular large capsule during the process of natural closure of a ventricular septal defect (VSD). Aneurysm of the interventricular membranous septum (AMS) is similar to anomalies of the tricuspid valve, including pouches, and misinterpretations appear in the literature. Complications such as rupture, endocarditis or thrombosis are unusual for either a tricuspid pouch or AMS? We report a patient with a large tricuspid pouch that we thought was AMS until cardiac surgery.

Case Report

A 63-year-old man was admitted to hospital because of left hemiplegia. Motor function of the left side was diminished, possibly as a sequel of a prior neurological accident (transient cerebral ischemic attack) 10 years ago and a more recent stroke. Brain computed tomography revealed a low-density area within the right lateral ventricle, which corresponded to the left paralysis.

Clinical examination revealed blood pressure of 120/70 mmHg, heart rate of 80 beats/min and respiratory rate of 15 breaths/min. Chest X-ray was normal and electrocardiogram (ECG) showed sinus rhythm and left ventricu-
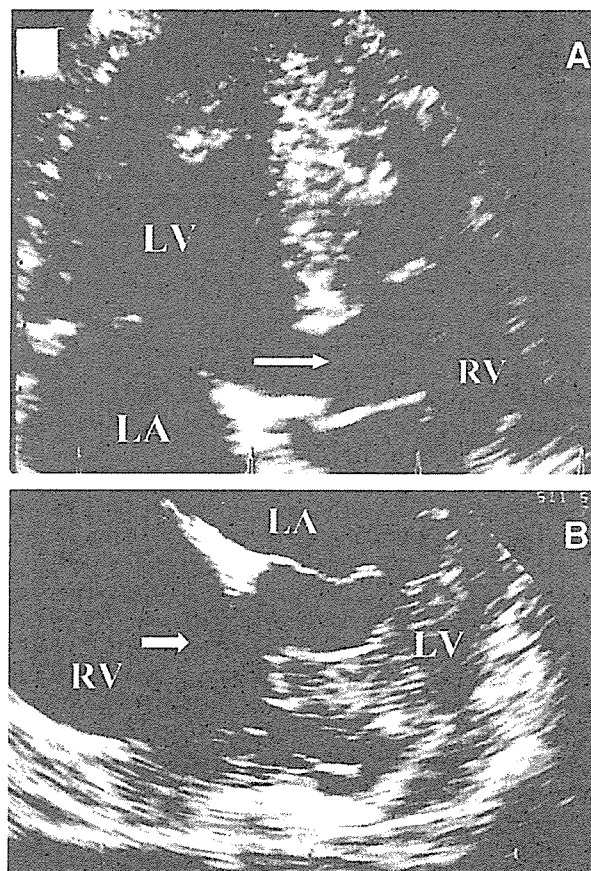

Fig 1. (A.B) Preoperative transthoracic and transesopageal echocardiograms in the 4-chamber view showing the tricuspid pouch at inflow of the right ventricle. LA, left atrium; LV, left ventricle; RV, right ventricule.
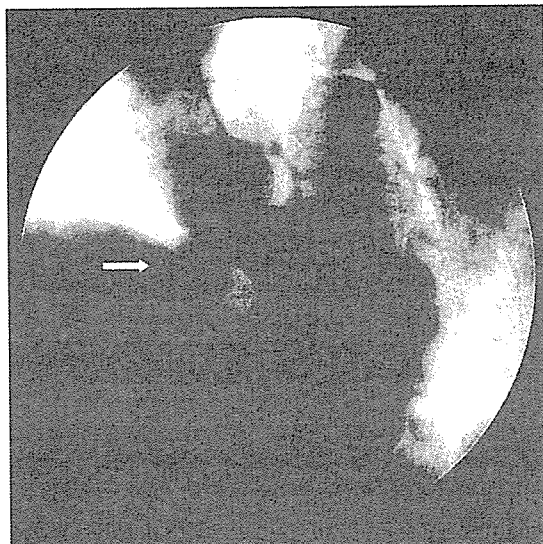
Fig 2. Left ventricular angiography in left anterior oblique view shows a pouch-like structure bulging into the right ventricle during sytole.
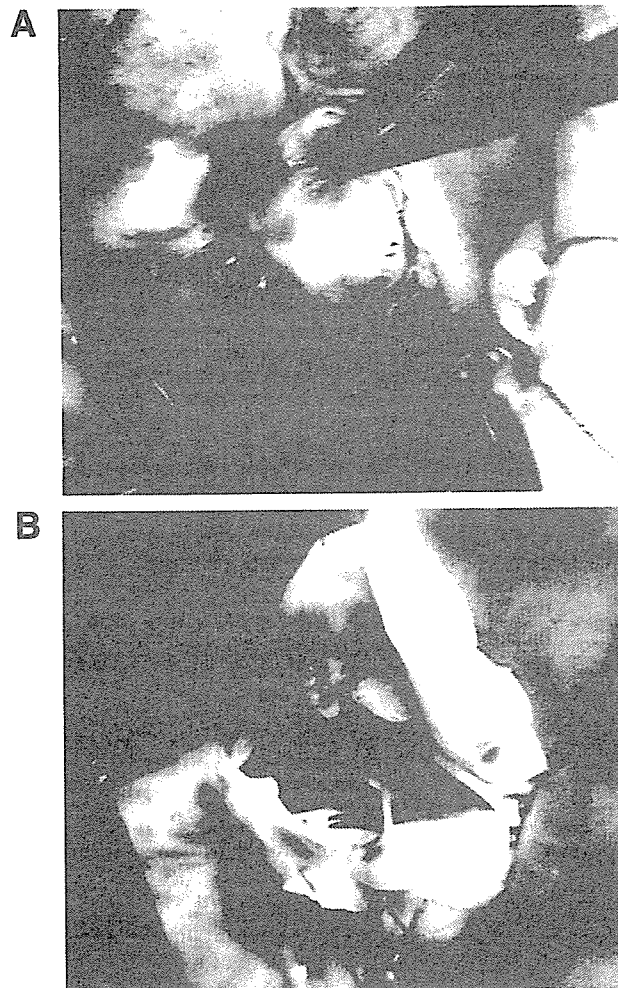

Fig 3. (A) Right atrium is opened to reveal a spherical aneurysmal pouch 2 cm in diameter and formed by the adherence of the septal leaflets. (B) Incision of the tricuspid leaflet exposes the true ventricular septal defect.

lar hypertrophic pattern. Transthoracic and transesophageal echocardiography (TEE) revealed an aneurysm protruding into the right ventricle (Fig 1A,B) with eddying of blood on TEE, but we did not recognize the thrombus in the pouch or its mobility. The findings of left ventricular angiography (LVG) in the left anterior oblique projection were similar to those for AMS (Fig 2). It protruded during inflow of the right ventricle and its surface was regular and cauliflower-like. There was no left-to-right shunt flow, no dilatation of the right ventricle and trivial tricuspid regurgitation. We could not confirm if the cerebral thrombosis had a cardiac origin or not, but brain magnetic resonance imaging suggested that the cerebral infarction had been caused by embolism because of the site and the sudden onset of hemiparesis. Therefore, we considered that the protruding aneurysm was the most likely culprit for blood stasis and thrombus formation and that cardiac operation was necessary to prevent stroke attack in the future.

At operation, besides a perimembranous outlet type of VSD, a pouch of 2.0 cm in diameter was found adjacent to the septal leaflet of the tricuspid valve (Figs 3A,B). There was not a residual membranous septum and the surface of right ventricle that was adhered to the septal leaflet was irregular and discolored. The tendon of the tricuspid valve was slightly extended. The VSD was closed with a patch. Based on these findings, we speculated that the tricuspid pouch was formed by the effect of a jet stream through the VSD.

After surgery, anticoagulant therapy was instituted for 3 months and to date the patient is healthy and has not had other neurological events.

Discussion

A pouch-like structure that bulges into the right ventricle on LVG is almost always considered to be AMS, which is a rare congenital lesion that is almost always associated with congenital anomalies such as VSD and endocardial cushion defect[3,4] Many investigators have reported the occurrence of AMS[2,5-7] but its mechanism of development is a matter of argument. Baron et al[2] reported that AMS is formed by

projection of left ventricular pressure during spontaneous closure of a VSD, which occurs in a significant percentage of patients, usually during infancy. Except for muscular defects, the mechanism of closure is not clearly understood. It may occur as a result of deposition of fibrin over the margins of the defect or by attachment to the septum of the septal leaflet of the tricuspid valve[1,6] In the presence of a VSD, left-to-right shunt flow jet toward the tricuspid valve may occur after adhesion of the septal leaflet of the tricuspid valve to the margin of the VSD. But this is not AMS, rather it is a tricuspid pouch. Idriss et al[3] reported that tricuspid pouch was occurred in 12.2% of cases of VSD. Tricuspid pouch sometimes causes subpulmonary obstruction in association with transposition of the great arteries, but rarely does so without transposition[8] Generally, the development of a tricuspid pouch is secondary to ineffective treatment of endocarditis. However, in the present patient, the surface of the tricuspid valve was smooth and there was no inflammatory change. The pouch was created by a jet lesion of the VSD. Tricuspid pouch can be confused with AMS and both are diagnosed by 2-dimensional echocardiography and LVG, although it is difficult to distinguish them before operation, as in the present case.

The clinical course of most cases of tricuspid pouch is

silent and complications, such as rupture, endocarditis or thrombosis, are unusual. In the present case, the pouch was not associated with interventricular communication and repeated cerebrovascular embolism occurred. The risk of thrombo-embolic complications for AMS and tricuspid pouch is almost same. In cases with a small or negligible VSD, conditions are favorable for blood stasis and thrombus formation. Thrombo-embolic complications with tricuspid pouch are very rare, but may be underestimated, as in the past with aneurysm of the interatrial septum, which was considered to be a potential cause of thrombo-embolism. Previous investigators have reported complications of AMS, such as cerebral infarction,[9-12] and all of these previous cases underwent surgery because there was possibility of thrombus in the future. A report of tricuspid pouch is rare because the final diagnosis of tricuspid pouch is made during cardiac surgery.

Rhythm disturbances have been reported in associated with AMS,[13] but none of the reported cases of AMS with thrombo-embolism had cardiac arrhythmias,[12] nor was there evidence of atrial fibrillation or ventricular premature contraction on Holter ECG in the present case.

We could not confirm thrombus in the aneurysm, but after the patient had had a transient ischemic attack approximately 10 years ago, he was administered aspirin and nevertheless he had another severe stroke. Surgical investigation for a tricuspid pouch is essential when cerebral embolism occurs despite anticoagulant therapy.

References

1. Hamby RI, Raia F, Apiado O. Aneurysm of the pars membranacea: Report of three adult cases and a review of the literature. *Am Heart J* 1970; **79:** 688–699.
2. Baron MG, Wolf BS, Grishman A, Van Mierop LHS. Aneurysm of the membranous septum. *Am J Roentgenol* 1964; **91:** 1303–1313.
3. Idriss FS, Muster AJ, Paul MH, Backer CL, Mavroudis C. Ventricular septal defect with ricuspid pouch with and without transposition: Anatomic and Surgical consideration. *Thorac Cardiovasc Surg* 1992; **103:** 52–59.
4. Kudo T, Yokoyama M, Iwai Y, Konno S, Sakakibara S. The tricuspid pouch in endocardial cushion defect. *Am Heart J* 1974; **87:** 544–549.
5. Rogers HM, Evans IC, Domeier LH. Congenital aneurysm of the membranous portion of the ventricular septum: Report of two cases. *Am J Pathol* 1952; **43:** 781–790.
6. Chesler E, Korns ME, Edwards JE. Anomalies of the tricuspid valve, including pouches, resembling aneurysm of the membranous ventricular septum. *Am J Cardiol* 1968; **21:** 661–668.
7. Varghese PJ, Izukawa T, Celermajer J, Simon S, Rowe RD. Aneurysm of the membranous ventricular septum: A method of spontaneous closure of small ventricular septal defect. *Am J Cardiol* 1969; **24:** 531–536.
8. Kaneko Y, Okabe H, Nagata N, Kanemoto S, Yamada S. Right ventricular obstruction by tricuspid pouch in simple ventricular septal defect. *Ann Thorac Surg* 1998; **65:** 550–551.
9. Bush HS, Perin E, Massumi A, Klima T, Hall RJ. Detection of thrombus in an aneurysm of the ventricular septum. *Am J Cardiol* 1989; **63:** 1533–1535.
10. Thomas D, Salloum J, Rancurel G. Aneurysm of the interventricular membranous septum with thrombo-embolism: An indication for surgical repair? *Eur Heart J* 1993; **14:** 1717–1718.
11. Lin JM, Hwang JJ, Chiu IS. Cerebral embolism from the thrombus in the atrioventricular septal aneurysm. *Cardiology* 1995; **86:** 441–443.
12. Salazar J, Gutierrez A, Cay E, Ballester C, Salazar JJ, Placer L. Cerebral embolism and thrombus in a membranous interventricular septal aneurysm. *Ann Thorac Surg* 2003; **76:** 286–287.
13. Langenfeld H, Meesmann M, Schanzenbaucher P. Angeborenes aneurysm des membranosen interventrikularen Septums. *Dtsch Med Wochenschr* 1990; **115:** 622–625.

Inhibition of protein phosphatase 1 by inhibitor-2 gene delivery ameliorates heart failure progression in genetic cardiomyopathy

Michio Yamada,[*,†] Yasuhiro Ikeda,[*,†,1] Masafumi Yano,[†] Koichi Yoshimura,[*] Shizuka Nishino,[*] Hidekazu Aoyama,[*,†] Lili Wang,[‡] Hiroki Aoki,[*] and Masunori Matsuzaki[*,†]

*Department of Molecular Cardiovascular Biology Yamaguchi University School of Medicine; †Department of Medicine and Clinical Science, Division of Cardiology, Yamaguchi University Graduate School of Medicine, Ube, Japan; and ‡Medical Genetics Division, Department of Medicine, University of Pennsylvania, Philadelphia, Pennsylvania, USA

To read the full text of this article, go to http://www.fasebj.org/cgi/doi/10.1096/fj.05-5299fje

SPECIFIC AIMS

Protein phosphatase 1 (pp1), the major isotype of Ser/Thr protein phosphatase in cardiomyocytes, has been shown to be overactivated in the cytosol and in the preparations of sarcoplasmic reticulum (SR) in diseased hearts, although the relationship between PP1 and protein kinase A (PKA) signaling during heart failure (HF) progression has not been clearly demonstrated. We hypothesized that hyperactive PP1 is a maladaptive mechanism that occurs in conjunction with altered PKA signaling during HF progression, and inhibition of PP1 by inhibitor-2(INH-2) may be favorable for preserving cardiac function in HF. In the present study, we first characterized disease-stage-related changes in PP1 activities together with the PKA activities and phosphorylation status of several key proteins, and we further investigated whether *in vivo* PP1 inhibition by gene transfer of INH-2 prevents HF progression in the cardiomyopathic (CM) hamster, a well-established genetic HF model, which harbors the same genetic deficiencies as human dilated cardiomyopathy.

PRINCIPAL FINDINGS

1. Adenoviral mediated INH-2 gene delivery improves contractility in cardiomyocytes via increase in phosphorylation of Ser-16-PLN

AdV-INH-2 gene transfer significantly inhibited PP1 activity in adult rat cardiomyocytes without any effect on PP2A activity. Following adenovirus transfection, INH-2 significantly increased the phosphorylation of phospholamtan (PLN) at Ser-16, and enhanced Ca^{2+} transients and % cell shortening.

2. *In vivo* adenovirus-mediated INH-2 gene delivery improves LV systolic function

We tested the effect of *in vivo* AdV-mediated high-efficiency cardiac gene transfer of INH-2 on cardiac dysfunction at 14 wk in the midst of the transition phase of HF from moderate to severe dysfunction. At 7 days after gene transfer, the INH-2-transfected hamsters showed a significant reduction in LV chamber size (LV end-diastolic dimension and LV end-systolic dimension; LVDd and LVDs) and an improvement of percent fractional shortening of the LV (%FS) (**Fig. 1**) compared with that before the gene transfer. Successful INH-2 gene transduction was confirmed by the immunoblotting for INH-2, as shown mainly in the cytosol. Interestingly, quantitative analysis revealed that the expression of INH-2 caused the changes in the subcellular distribution of PP1 catalytic subunit (PP1C) in the myocardium after the *in vivo* gene transfer. High level of INH-2 expression was accompanied with a higher amount of cytosolic PP1C than that in the LacZ-treated group, without inducing the corresponding increase in cytosolic PP1 activity. In contrast, higher INH-2 expression was accompanied with lower amount of microsomal PP1C and lower microsomal PP1 activity compared with that in the LacZ-treated group. Because INH-2 was found exclusively in the cytosol, these findings are interpreted that INH-2 induced an increase in inactive PP1C pools in the cytosol, thereby decreasing the active PP1C in the microsomes. This may account for the increase in phospho-Ser-16 PLN after *in vivo* INH-2 gene transfer (**Fig. 2**).

---

[1] Correspondence: Department of Molecular Cardiovascular Biology, Yamaguchi University School of Medicine, 1-1-1 Minami-Kogushi, Ube 755-8505 Japan. E-mail: ysikeda @yamaguchi-u.ac.jp
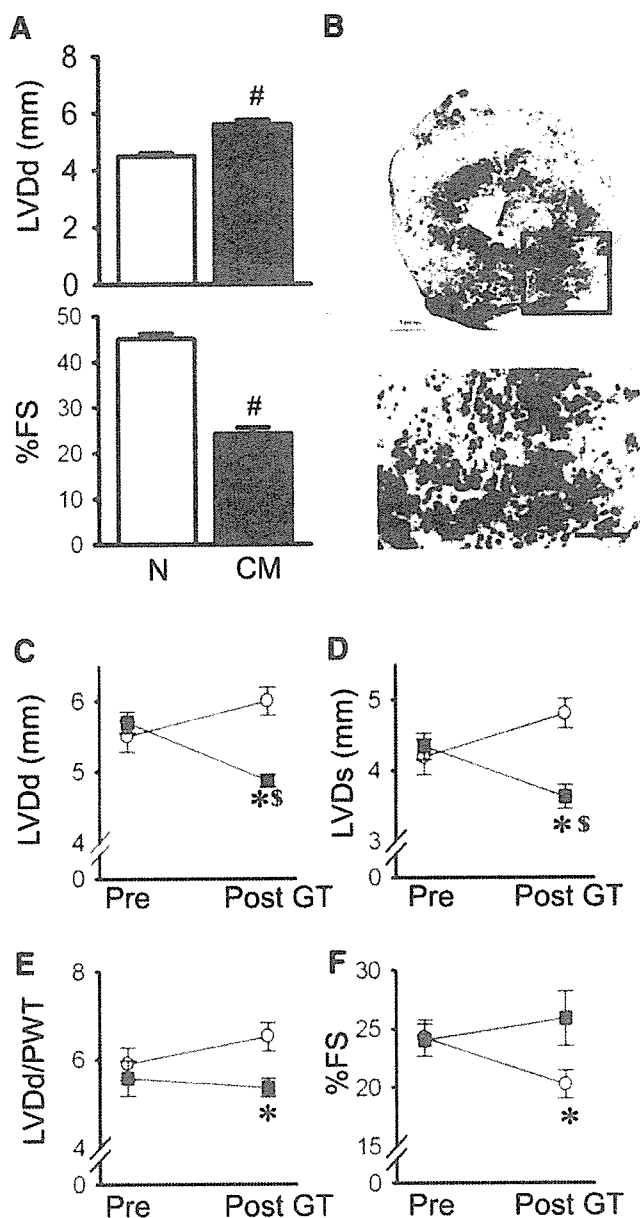doi: 10.1096/fj.05-5299fje

Figure 1. *In vivo* AdV-INH-2 gene transfer improves LV systolic function in cardiomyopathic (CM) hamsters. *A)* The left ventricular (LV) end-diastolic dimension (LVDd) and percent fractional shortening (%FS) at 14 wk of age are shown for normal (N) and CM hamsters (*n*=10 in each group). #*P* < 0.05 compared with normal hamsters. *B)* Representative Bluo-gal staining is shown at 7 days after AdV-LacZ gene transfer in a CM hamster. High magnification of the rectangular area is shown (*bottom*). *C)* The LV end-diastolic and systolic dimensions (LVDd, LVDs) are shown for CM hamsters at 7 days after the gene transfer (GT) of LacZ (open circles, *n*=8) or INH-2 (solid squares, *n*=8). The index of wall stress, LVDd/PWT and the changes of %FS are shown for the gene transfer of LacZ (open circles) and INH-2 (solid squares). **P* < 0.05 compared with LacZ-treated hamsters. $*P* < 0.05 compared with pre gene transfer.

On the other hand, phosphorylation of ryanodine receptor (RyR) at Ser-2808 did not show significant change, and another intracellular PKA phosphorylation target, CREB, did not show any change in phosphorylation at Ser-133 by INH-2 gene transfer com-

pared with the LacZ-treated group. The level of PKA activity in CM hamster heart at 14 wk was significantly higher than either the level of baseline PKA activity or that of maximally stimulated state by intravenous (i.v.) isoproterenol infusion in normal hamsters. Interestingly, INH-2 gene transfer significantly prevented an abnormal increase in PKA activity, although it did not affect the increase in PLN phosphorylation at Ser-16. Decrease in PKA activity in INH-2 treated hamsters paralleled with a decreasing trend in plasma catecholamine levels, suggesting that the reduction in the PKA activity was due to a decrease in sympathetic drive. Gene delivery of INH-2 into the CM hamster heart reduced brain natriuretic peptide (BNP) levels, a predictor of exacerbation of HF, compared with the LacZ-treated group. These results indicate that INH-2 gene transfer has a favorable effect on the failing heart, over the short term.

3. *In vivo* adeno-associated virus-2-(AAV-) mediated INH-2 gene delivery improves LV systolic function and extends survival time

Since *in vivo* AdV-INH-2 gene delivery resulted in improvement of cardiac function and ameliorated BNP expression over the short term, we further tested the long-term effect of INH-2 gene delivery by AAV-mediated gene transfer. We performed AAV-mediated gene transfer of INH-2 at 14 wk of age, followed by serial assessment of cardiac function for 12 wk after the gene transfer by echocardiography and hemodynamic analysis. AAV-INH-2 gene transfer preserved %FS with persistent suppression of microsomal PP1 activity and increased PLN phosphorylation at Ser-16 compared
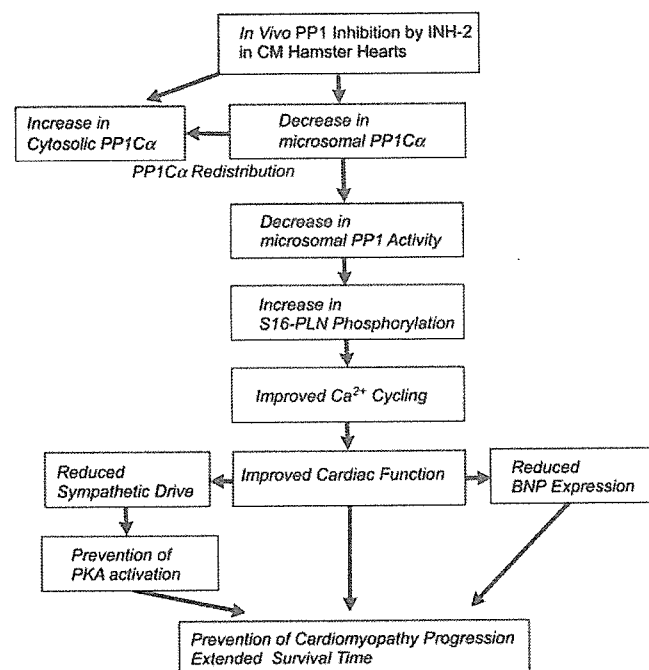

Figure 2. Schematic diagram for *in vivo* cardiac PP1 inhibition by INH-2 in CM hamsters
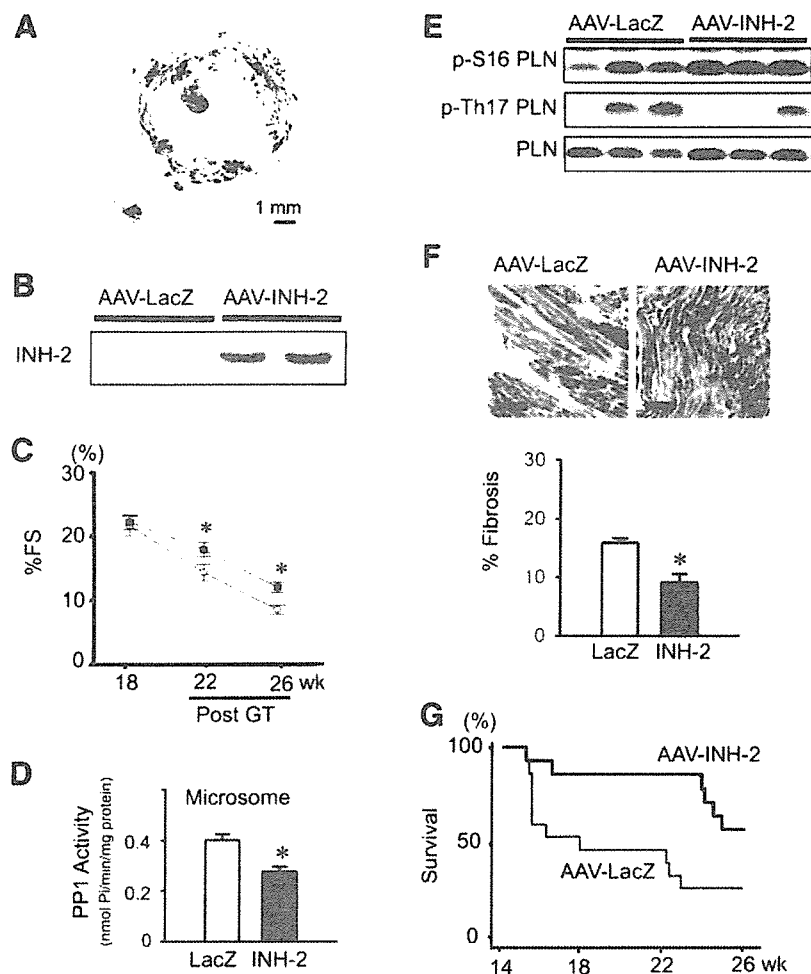
Figure 3. Effects of AAV-INH-2 gene transfer on cardiac function and survival time course in CM hamsters. A) Representative Bluo-gal staining is shown for the LV cross section at 12 wk after AAV-LacZ gene transfer. B) A representative immunoblot is shown for INH-2 at 12 wk after AAV-LacZ gene transfer. C) The time course of %FS (%fibrous sheath) assessed by echocardiography is shown for the LacZ group (open circles) and INH-2 group (solid squares) gene transfer by AAV. *$P < 0.05$ compared with the LacZ group. D) Microsomal PP1 activity is shown after AAV-mediated gene transfer into the hearts of the LacZ ($n=5$) and INH-2 groups ($n=7$). *$P < 0.05$ compared with the LacZ-treated group. E) Representative immunoblottings are shown for Ser-16 PLN, Thr17 PLN, and total PLN in the LacZ-treated ($n=4$) and INH-2-treated ($n=4$) groups. F) Representative images are shown from tissue sections with Azan Mallory staining from the LacZ-treated ($n=6$) and INH-2-treated ($n=7$) CM hamsters. Quantification of the percent areas of fibrosis are shown (*bottom*). *$P < 0.05$ compared with the LacZ-treated group. G) The Kaplan-Meier plot is shown for the survival of CM hamsters after AAV-mediated gene transfer of LacZ ($n=17$) and INH-2 ($n=13$) ($P = 0.03$).

with the AAV-LacZ-treated group over the observation period (**Fig. 3**). In addition, INH-2-treated hamster heart showed less interstitial fibrosis compared with that in LacZ-treated hearts. In the Kaplan-Meier plot, the AAV-INH-2-treated group showed a 54% survival rate at 12 wk after the gene transfer, whereas the AAV-LacZ-treated CM hamsters exhibited a deleterious time course, ending with a 29% survival rate. The difference between these survival curves was statistically significant ($P = 0.03$). These results clearly indicate that INH-2 gene transfer had a favorable effect on progressive HF in the long term.

CONCLUSIONS AND SIGNIFICANCE

In the present study, we demonstrated that *in vivo* gene transfer of INH-2 effectively prevented HF progression throughout the one-week observation period in the experiment using adenoviral gene transfer and throughout three-month observation period in the experiment using AAV-mediated gene transfer. The INH-2 gene transfer not only preserved LV function but also reduced mRNA expression of

BNP, a prognostic marker of HF, in the short-term experiment. Furthermore, long-term expression of exogenous INH-2 also slowed the progression of LV dysfunction and extended survival in CM hamsters. To our knowledge, this is the first report demonstrating the long-term therapeutic effect of PP1 inhibition in progressive HF using a high-efficiency cardiac gene transfer approach.

Our data suggested that the beneficial effect of INH-2 gene delivery is, at least in part, attributable to the increase in phosphorylation of PLN at Ser-16 (Fig. 2), because inhibition of endogenous PLN has been reported to be beneficial in treating certain types of HF, including HF in the other hamster model of cardiomyopathy (i.e., the BIO14.6 strain model).

In conclusion, we have demonstrated that *in vivo* myocardial PP1 inhibition by inhibitor-2 up-regulated SR calcium handling through PLN phosphorylation and protected cardiomyocyte damage, thereby ameliorating the long-term progression of HF in the cardiomyopathic hamster. Modulation of PP1 activity by INH-2 may constitute a new therapeutic strategy for the treatment of end-stage HF. [FJ]

Inhibition of protein phosphatase 1 by inhibitor-2 gene delivery ameliorates heart failure progression in genetic cardiomyopathy

Michio Yamada,[*,†] Yasuhiro Ikeda,[*,†,1] Masafumi Yano,[†] Koichi Yoshimura,[*] Shizuka Nishino,[*] Hidekazu Aoyama,[*,†] Lili Wang,[‡] Hiroki Aoki,[*] and Masunori Matsuzaki,[*,†]

*Department of Molecular Cardiovascular Biology Yamaguchi University School of Medicine; †Department of Medicine and Clinical Science, Division of Cardiology, Yamaguchi University Graduate School of Medicine, Ube, Japan; and ‡Medical Genetics Division, Department of Medicine, University of Pennsylvania, Philadelphia, Pennsylvania, USA

ABSTRACT   The type 1 protein phosphatase (PP1) has been reported to be overactivated in the failing heart, leading to a depression in cardiac function. We investigated whether *in vivo* PP1 inhibition by myocardial gene transfer of inhibitor-2 (INH-2), an endogenous PP1 inhibitor, alleviates heart failure (HF) progression in the cardiomyopathic (CM) hamster, a well-established HF model. Adenoviral INH-2 gene delivery improved % fractional shortening of the left ventricle (LV) accompanied by reduced chamber size at 1 wk. *In vivo* myocardial INH-2 gene delivery induced an increase in cytosolic PP1 catalytic subunit α (PP1Cα) without inducing the corresponding increase in cytosolic PP1 activity. On the other hand, INH-2 delivery induced a decrease in microsomal PP1Cα, resulting in a preferential decrease in microsomal PP1 activity, thereby increasing in phospholamban phosphorylation at Ser16. INH-2 gene transfer alleviated brain natriuretic peptide expression, presumably reflecting improved cardiac function. Moreover, adeno-associated virus-mediated INH-2 gene delivery significantly extended the survival time for 3 mo. These results indicate that increased PP1 activity is an exacerbating factor during progression of genetic cardiomyopathy and modulation of PP1 activity by INH-2 provides a potential new treatment for HF without activating protein kinase A signaling in cardiomyocytes.— Yamada, M., Ikeda, Y., Yano, M., Yoshimura, K., Nishino, S., Aoyama, H., Wang, L., Aoki, H., and Matsuzaki, M. Inhibition of protein phosphatase 1 by inhibitor-2 gene delivery ameliorates heart failure progression in genetic cardiomyopathy. *FASEB J.* 20, E346–E356 (2006)

Key Words: gene transfer • protein kinase A • phosphorylation • phospholamban

HEART FAILURE (HF) is a leading cause of death in developed countries. Morbidity and mortality rates remain high despite the recent significant progress in medical and surgical therapy (1). Development of a new therapeutic strategy, which will complement the underlying biological process within the failing heart is awaited to alleviate the high mortality in patients with HF.

In this context, recent studies have revealed that defective regulation of Ca^{2+} cycling in the failing heart is a major determinant of progressive cardiac dysfunction and fatal arrhythmia (2, 3). Importantly, the amplitude and the velocity of Ca^{2+} cycling in cardiomyocytes are finely regulated by dynamic balance of phosphorylation and dephosphorylation through kinases and phosphatases in response to a variety of extrinsic stimuli. For example, sympathetic stimulation leads to activation of the β-adrenergic receptor, which, in turn, stimulates the production of cyclic AMP (cAMP) by adenylate cyclase, resulting in the activation of protein kinase A (PKA). Activated PKA phosphorylates phospholamban (PLN) and ryanodine receptor (RyR) in the sarcoplasmic reticulum (SR), thereby augmenting the amplitude and the velocity of SR Ca^{2+} cycling and cellular contractility (4) in a beat-by-beat manner, whereas protein phosphatase (PP)1 and 2A counterbalance phosphorylation of these proteins (5).

In the failing heart, chronic overactivation of the β-adrenergic system leads to maladaptation of these cellular signaling via PKA hyperactivation with hyperphosphorylation of RyR (6) and/or hyperactivation of protein phosphatases with hypophosphorylation of PLN (7, 8) in the corresponding subcellular domain. These abnormalities cause impaired sarcoplasmic reticulum (SR) Ca^{2+} loading and cytosolic Ca^{2+} overload, resulting in myocyte damage.

Protein phosphatase 1 (PP1), the major isotype of Ser/Thr protein phosphatase in cardiomyocytes (5), has been shown to be overactivated in the cytosol and

in the preparations of SR in diseased hearts, (7, 9–11), although the relationship between PP1 and PKA signaling during HF progression has not been clearly demonstrated. The role of PP1 hyperactivity is also supported by the finding of Carr et al. (12) that overexpression of the PP1 catalytic subunit α (PP1Cα) in the mouse heart caused dilated cardiomyopathy. In this regard, overexpression of inhibitor-1 (INH-1), an endogenous PP1 inhibitor, or constitutively active INH-1 has been shown to restore Ca^{2+} cycling and cell contraction/relaxation in *in vitro* cardiomyocytes (12, 13) and *in vivo* aorta-constricted rat hearts (14). In addition, inhibitor-2 (INH-2), another endogenous PP1 inhibitor, has also been shown to increase cardiac contractility by augmenting Ca^{2+} cycling in a transgenic model (15).

Accordingly, we hypothesized that hyperactive PP1 is a maladaptation mechanism in conjunction with altered PKA signaling during HF progression, and inhibition of PP1 by INH-2 may be favorable for preserving cardiac function in HF. In the present study, we first characterized disease stage-related changes in PP1 activities together with PKA activities and phosphorylation status of several key proteins. We further investigated whether *in vivo* PP1 inhibition by gene transfer of INH-2 prevents HF progression in the cardiomyopathic (CM) hamster, a well-established genetic HF model which harbors the same genetic deficiency as human dilated cardiomyopathy (16, 17).

MATERIALS AND METHODS

Animals

Animal experiments were carried out on normal male hamsters (6 to 28 wk old) obtained from Japan SLC and UMX7.1 CM hamsters bred at Yamaguchi University. Male adult rats (8 wk old) for isolation of adult rat cardiomyocyte were obtained from Japan SLC. All animal protocols were approved by the Yamaguchi University School of Medicine Animal Subject Committee.

Hemodynamic measurement

Hamsters of three different ages (6, 10, and 28 wk old) underwent transthoracic echocardiography and left ventricular (LV) pressure measurement as described previously (18, 19). Briefly, hamsters were anesthetized by an intraperitoneal (i.p.) injection of sodium pentobarbital (50 mg/kg), followed by measurement of LV diameter by a HDI-5000 ultrasound machine (Philips, Netherlands) equipped with a 15-MHz probe. Pressure in the LV was measured using a fidelity pressure manometer (Millar, Houston, TX) introduced through the LV apex by a small midline thoracotomy. Maximum and minimum LV dP/d*t* and the time constant of relaxation, τ (using an exponential function), were calculated from LV pressure as described (20).

Cell fractionation and immunoblottings

The LV specimens were homogenized with the buffer containing (in mM): 25 Tris-HCl (pH 7.4), 50 NaCl, 300 sucrose,

1 EDTA, 1 EGTA, 50 NaF, 1 Na_3VO_4, 1% Nonidet P-40, 0.5% deoxycholic acid, 0.1% SDS, 0.02% 2-mercaptoethanol, as well as 1% protease inhibitor cocktail (PIC) (Sigma, St. Louis, MO). Protein concentrations were calibrated by Bradford assay, and an equal amount of samples was loaded onto each lane for quantitative immunoblot analysis by using LAS-1000 (Fuji-Film, Tokyo, Japan). Part of the LV specimens underwent subcellular fractionation to obtain cytosolic and microsomal fractions, as described previously (19) in the buffer containing (in mM): 25 Tris-HCl (pH 7.4), 50 NaCl, 300 sucrose, 1 EDTA, 1 EGTA, 50 NaF, 1 Na_3VO_4, as well as 0.02% 2-mercaptoethanol and 1% PIC.

Protein phosphatase activities

Specimens for PP assay were prepared from both the cytosol and the microsome fraction in the buffer containing (in mM):25 Tris-HCl (pH7.4), 50 NaCl, 300 sucrose, 0.1 EDTA, 0.1 EGTA, 1% Triton-X 100 0.02% 2-mercaptoethanol, and 1% PIC. The PP1 activity was measured in the absence or presence of 1 nM okadaic acid (OA) to block PP2A activity or 1 μM OA to block both PP1 and PP2A activities with [^{32}P]phosphorylase *a* as a substrate (21). The specificity of measurement for PP1 activity with use of 1 nM OA was confirmed by addition of 500 nM recombinant inhibitor-2 peptide (Sigma) to block entire PP1 activity into the reaction solution.

Protein kinase A activity, cyclic AMP content, and plasma catecholamine measurements

The PKA activity was measured from the LV homogenates using a kit (V7480; Promega, Madison, WI) according to the manufacturer's instructions. The plasma norepinephrine, epinephrine, and tissue cyclic AMP levels were measured as described previously (22). The tissue homogenates from isoproterenol-stimulated hearts were prepared as described previously (23).

Construction of adenoviruses and adeno-associated viruses

Recombinant human adenovirus-5 (AdV) encoding nuclear localizing β-galactosidase (LacZ) was amplified and purified as described previously (20). The human INH-2 cDNA (NM_006241) was amplified by RT-PCR with the primer set of 5′-GCAGAATTCACCATGGCGGCCTCGACGGCCTCG-3′ and 5′-GCATCTAGATGAACTTCGTAATTTGTTTTGCTG-3′. The adenovirus encoding INH-2 was created with or without a FLAG tag at the carboxyl-terminal, amplified, and purified as described previously (20). Recombinant adeno-associated virus serotype-2 vectors (AAV) encoding LacZ or INH-2 were produced in the vector core facility at the University of Pennsylvania.

Analysis of isolated adult rat cardiomyocytes

Adult rat cardiomyocytes were prepared from 8-wk-old Wistar rats, as described previously (24). Isolated rat cardiomyocytes were transfected with AdV at an MOI of 100 and incubated for 36 h at 37°C in 5%CO_2/95%O_2 atmosphere. Cardiomyocyte shortening and intracellular Ca^{2+} transients were simultaneously recorded, as described previously (25). A total of 40 cells were analyzed from 8 wk-old male Wistar rats.

Cardiac *in vivo* AdV/AAV transfection protocol

Fourteen-week-old male normal and CM hamsters underwent *in vivo* high-efficiency cardiac gene delivery, according to the

previously described protocol (20). Briefly, preoperative echocardiography was performed in all animals, hamsters were anesthetized with sodium pentobarbital (75 mg/kg), and ventilated, and the right carotid artery was cannulated with a catheter placed at the aortic root. The animals were subjected to general hypothermia by external cooling until the core temperature reached below 26°C. The pulmonary artery and the ascending aorta were occluded, histamine pretreatment was administered into the aorta (20 mM, vol 2.5 µl/gram body wt for 3 min), followed by the injection of the viral vector solution and subsequent resuscitation. A total of 1–6 × 10^{11} viral particles of AdV or AAV particles per 100 g of body wt were injected through the transcoronary route. The animals were terminated at 7 days after gene transfer in the AdV protocol, and at 12 wk after gene transfer in the AAV protocol.

The number of operated animals was as follows: normal hamsters, $n = 6$ for AdV-LacZ and $n = 6$ for AdV-INH-2; CM hamsters, $n = 20$ for AdV-LacZ, $n = 20$ for AdV-INH-2, $n = 20$ for AAV-LacZ, and $n = 17$ for AAV-INH-2 Death of the animals within 5 days after gene transfer procedure was regarded as improper recovery and not incorporated into the survival study (AAV-LacZ-treated group; $n=3$, AAV-INH-2-treated group, $n=4$). Overall operational mortality in 14-week-old CM hamsters subjected to the hypothermic gene delivery by AdV or AAV vectors was 18%.

Postgene transfer analysis

Before termination, the left ventricular dimension and systolic function were assessed in all animals with echocardiography and hemodynamic measurement by an operator who was unaware of the transduced gene. The heart tissue was then acquired for biochemical analyses. The gene transfer efficiency was estimated in AdV-LacZ- or AAV-LacZ-treated hearts, as described previously (20). Total RNA was prepared by using an RNeasy kit (Qiagen, Hilden, Germany). Northern blot analysis and real-time RT-PCR (Roche Diagnostics, Basel, Switzerland) were performed as described previously (26). The RT-PCR primer sets for PP1Cα and GAPDH were (5'-TCTGACCCTGACAAGGATG-3', 5'-CTTCTACAACCTGAT-GTGCTC-3') and (5'-TGCGGAAGAAAACTGCCTGG-3', 5'-CGGCTTGGTAAGAAGTCAGACG-3'), respectively.

Antibodies

Antibodies for PP1Cα and Rho-GDI (BD Biosciences, San Jose, CA), PP1 catalytic subunit β (PP1Cβ) and INH-2 (Calbiochem), phosphorylated-PLN at Ser16, PLN and phosphorylated-cyclic AMP response element binding protein (CREB) at Ser133 (Upstate Biotechnology, Lake Placid, NY), phosphorylated-PLN at Thr17 (Badrilla, UK), RyR(Sigma), CREB(Cell Signaling Technology, Beverly, MA), were obtained from commercially available sources. An antibody (Ab) for phosphorylated-RyR at Ser2808 was generously provided by Dr. Marks, Columbia University. Ab for INH-1 was generated by immunizing New Zealand White rabbits with polypeptides (DNSPRKIQFTVPLLEC and CGEEPEGATESTGNQE) of rat INH-1, and affinity-purified with the peptides.

Statistical analysis

Comparisons between two groups were performed by Student's t test. Comparisons between repeated measurements were done by ANOVA, followed by post hoc testing (the Student-Newman-Keuls method was used to compare the two groups when appropriate). The cumulative survival curve was plotted by the Kaplan-Meier method, and statistical differ-

ence was evaluated by a log-rank test. A value of $P < 0.05$ was considered statistically significant. Data are expressed as the mean ± SEM

RESULTS

PP1 activities in CM hamster hearts

The time course of LV function was assessed by serial echocardiography, as shown in **Fig. 1**. CM hamsters showed almost normal cardiac function at 6 wk with normal LV pressure (Fig. 1A–C). At 10 wk, % fractional shortening (%FS) started to show a significant decrease, indicating progression of LV dysfunction. At 28 wk, LV diastolic dimension (LVDd) was markedly dilated with severe depression of %FS, decrease in LV systolic pressure, and elevation of LV end-diastolic pressure (Fig. 1A–C), indicating overt signs of HF.

Biochemical analyses were performed at 6, 10, and 28 wk for the PP activities (Fig. 1D–E) and PP1-associated protein expressions in the cytosol (Fig. 1F) and the microsome (Fig. 1G), respectively, and to determine the phosphorylation levels of key phosphoproteins in normal and CM hamsters (**Fig. 2**). CM hamsters showed a gradual increase in PP1 activity both in the cytosol (Fig. 1D) and in the microsome (Fig. 1E) over the course of disease, while there was no change in normal hamsters. There was no change in PP2A activity in CM hamster throughout the observation period (Supplemental Fig. 1A–B). Immunoblotting of PP1 isoforms revealed a significant increase in PP1Cβ (Fig. 1F and Supplemental Fig. 1D) in the cytosol throughout the observation period. Increased expression levels of PP1Cα and β in the microsome showed a trend to increase at 6 and 10 wk and significantly increased at 28 wk (Fig. 1G and Supplemental Fig. 1E–F). INH-1 expression in CM hamsters was decreased compared with that in age-matched normal hamsters throughout the observation period, and there was no change in INH-2 expression compared with normal hamsters or among the different age groups (Supplemental Figs. 1G–H and 2). These results suggest that increased expression levels of PP1Cs may account for the increase in the PP1 activity in each fraction, and other regulatory molecules, including INH-1 and INH-2 may play an additional role.

The phosphorylation levels of PLN at Ser16 and RyR at Ser2808 (27) (corresponding to the Ser2809 RyR reported by Reiken et al. (28)) declined over the time course in normal hamsters (Fig. 2). Despite the increase in PP1 activity, the phosphorylation levels of PLN at Ser16 and RyR at Ser2808 were increased at 10 wk, a period of compensatory LV dysfunction, in CM hamsters compared to those in the age-matched normal hamsters. Phosphorylation levels of PLN at Ser16 further decreased at 28 wk compared to those assessed at 6 and 10 wk in the same strain (Fig. 2A and 2B), and became insignificant compared to that in age-matched normal hamsters. Phosphorylation levels of RyR at
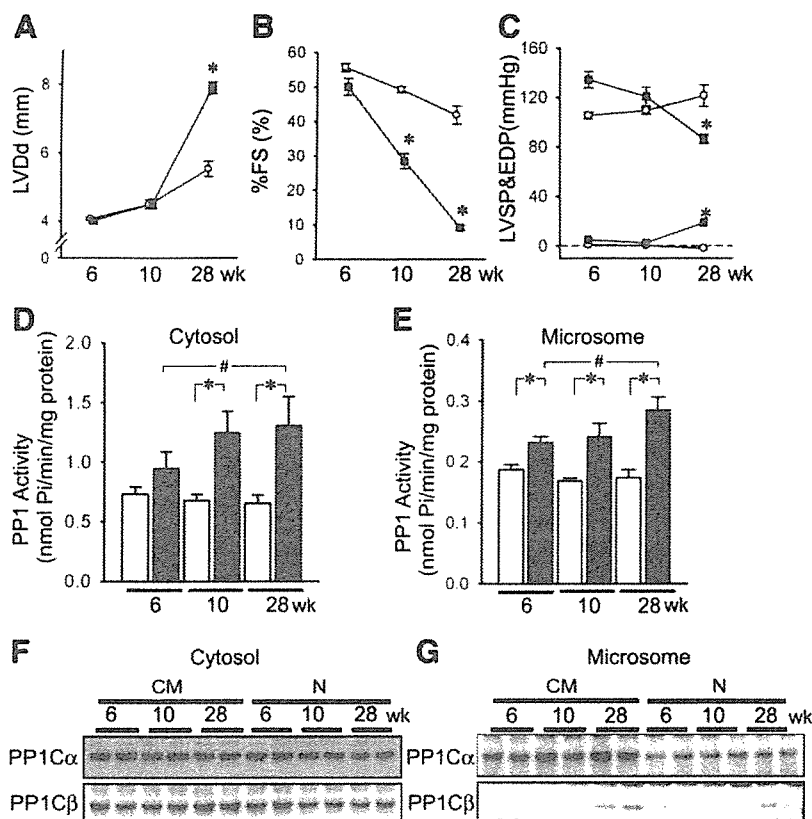
Figure 1. Increased protein phosphatase 1 (PP1) activity during the transition from cardiac dysfunction to heart failure (HF). A) Left ventricular end-diastolic dimension (LVDd). B) Percent fractional shortening of the LV(%FS). C) The LV peak systolic (SP) and end-diastolic pressure (EDP) are shown for normal (open circles, $n=6$) and cardiomyopathic (CM) hamsters(solid squares, $n=6$). The PP1 activities in the cytosol (D) and in the microsome (E) are shown for CM hamsters (solid columns, $n=6$) and age-matched normal hamsters (open columns, $n=6$). F, G) Representative immunoblots of PP1 catalytic subunits α(PP1Cα) and β(PP1Cβ) in CM hamsters and age-matched normal hamsters $n=6$ at 6, 10, and 28 wk of age in the cytosol (F) and in the microsomes (G). $*P < 0.05$ compared with age-matched normal hamsters. $\#P < 0.05$ compared with 6-wk-old hamsters of the same strain.

Ser2808 also showed a declining pattern at 28 wk (Fig. 2A and 2D) but still significantly higher than that in age-matched normal hamsters. Phosphorylation of PLN at Thr17 did not change significantly throughout the observation period between CM and normal hamsters or among the different age groups (Fig. 2A and 2C), although the phosphorylation showed a tendency to increase at 6 wk and a tendency to decrease at 28 wk in CM hamsters compared with normal hamsters. Phosphorylation of CREB at Ser133 in CM hamsters was decreased at 6 wk and became insignificant at 10 and 28 wk compared with that in normal hamsters (Fig. 2A and 2E). As phosphorylation of Ser16 PLN and of Ser2808 RyR was increased despite the increase in PP1 activity in CM hamsters, we hypothesized that PKA is hyperactive in CM hamster hearts. Indeed, the increases in phosphorylation of PLN at Ser16 and RyR at 2808 were roughly correlated with increased PKA activity (Fig. 2F) and cAMP content (Fig. 2G) during the transition to HF, whereas other phosphorylation targets such as Thr17 of PLN or Ser133 of CREB did not correlate with PKA activity. These data suggest that phosphorylation levels in Ser16-PLN and Ser2808-RyR are largely affected by the balance between PKA and PP1 activity during a period of compensatory LV dysfunction.

In vitro evaluation of overexpressing INH-2 in isolated adult cardiomyocytes
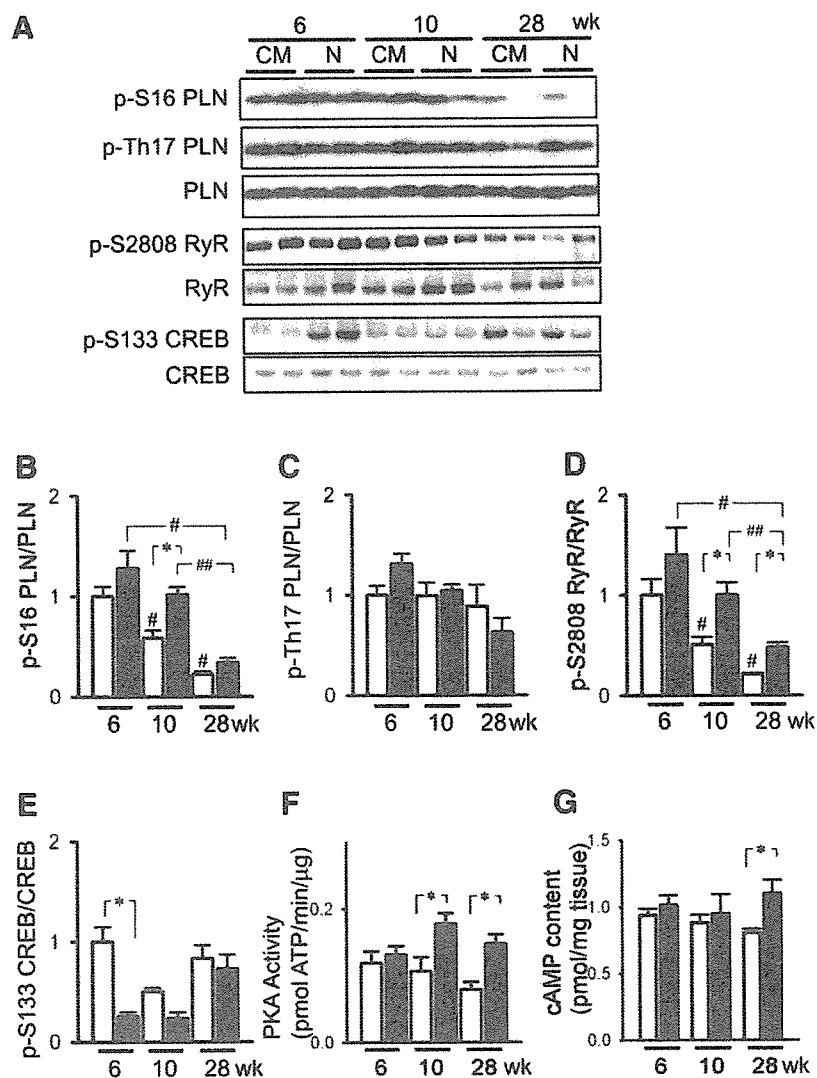
We used adenovirus (AdV)-mediated overexpression of INH-2 in cardiomyocytes to inhibit PP1 activity. Transduced INH-2 was detected in the cytosol in adult rat

cardiomyocytes (Fig. 3A). AdV-INH-2 gene transfer significantly inhibited PP1 activity without any effect on PP2A activity (Fig. 3B). There was no change in PP1C expression with INH-2 overexpression in cardiomyocytes (Fig. 3C). INH-2 gene transfer significantly increased the phosphorylation of PLN at Ser16 and of RyR at Ser2808 (Fig. 3C), and enhanced Ca^{2+} transients and % cell shortening, as shown in the representative traces (Fig. 3D) and summarized in Figure 3E. INH-2 induced a 2.2- fold increase in % cell shortening, along with augmentation of the Ca^{2+} amplitude and decay time constant of the descending limb of the Ca^{2+} transient. These results indicate that INH-2 gene transfer can efficiently modulate the PP1 activity in cardiomyocytes.

In vivo effect of AdV-INH-2 gene transfer on cardiac function

We first tested the effect of in vivo AdV-mediated high efficiency cardiac gene transfer of INH-2 on cardiac function in normal hamsters. Hamsters into which the INH-2 gene was transferred showed hypercontractile LV function compared with LacZ-treated hamsters (Fig. 4A). Successful INH-2 gene transduction was demonstrated by immunoblotting for INH-2, as shown in the cytosol (Fig. 4B). Interestingly, expression of exogenous INH-2 caused a 120% increase in cytosolic PP1Cα and a 63% decrease in microsomal PP1Cα (Fig. 4B). Although the expression of exogenous INH-2 caused an increase in cytosolic PP1Cα protein levels, there was no increase in cytosolic PP1 activity compared with the

A

	6		10		28 wk	
	CM	N	CM	N	CM	N

p-S16 PLN

p-Th17 PLN

PLN

p-S2808 RyR

RyR

p-S133 CREB

CREB

Figure 2. Expression and phosphorylation status of PP1-associated phosphoproteins in normal and CM hamster hearts. *A)* Representative immunoblots of phosphorylated PLN at Ser16 (p-S16 PLN), phosphorylated PLN at Thr17 (p-Th17 PLN), total PLN, phosphorylated RyR at Ser2808 (p-S2808 RyR), total RyR, phosphorylated CREB at Ser133 (p-S133 CREB), and total CREB are shown by immunoblotting of whole cell homogenate with quantitative analysis in *B–E.* The results of the quantitative analysis are expressed relative to the value in normal hamsters at 6 wk, which was designated as 1 (*n*=8 in each group). Endogenous protein kinase A (PKA) activities (*F*) and the concentrations of cyclic AMP (*G*) were measured in CM and normal hamsters (*n*=6 in each group). **P* < 0.05 compared with age-matched normal hamsters. # and *##P* < 0.05 compared with 6-week-old and 10-wk-old hamsters of the same strain, respectively.

B p-S16 PLN/PLN — 6 10 28wk

C p-Th17 PLN/PLN — 6 10 28wk

D p-S2808 RyR/RyR — 6 10 28 wk

E p-S133 CREB/CREB — 6 10 28 wk

F PKA Activity (pmol ATP/min/μg) — 6 10 28 wk

G cAMP content (pmol/mg tissue) — 6 10 28wk

LacZ-treated group, suggesting that INH-2 inhibits PP1C in the cytosol. Indeed, the expression levels of exogenous INH-2 showed an inverse correlation with the cytosolic PP1 activity within the INH-2 treated group (Supplemental Fig. 3*A*). In contrast, the 63% decrease in microsomal PP1Cα expression coincided with a 47% decrease in microsomal PP1 activity and an increase in PLN phosphorylation at Ser16 after INH-2 gene delivery (Fig. 4*B–D* and Supplemental Fig. 3*C–F*). These data suggest that overexpressed INH-2 induced an increase in inactive PP1Ca pools in the cytosol and promoted a translocation of active PP1Cα from the microsomes to the cytosol. These changes account for the decrease in microsomal PP1 activity, and concurrent increase in PLN phosphorylation at Ser16.

INH-2- gene transfer in CM hamsters was performed at 14 wk in the midst of the transition phase of HF from moderate to severe dysfunction. We chose this time point for the *in vivo* gene transfer study in order to test whether *in vivo* inhibition of PP1 is effective in preserving cardiac function after cardiac dysfunction becomes overt. At 14 wk, the CM hamsters showed a marked decrease in %FS and dilation in LVDd, as assessed by echocardiography (**Fig. 5***A*). We evaluated a total of 40

CM hamsters at 14 wk by echocardiography and randomly assigned them into two groups (20 CM hamsters received AdV-LacZ treatment and 20 received AdV-INH-2 treatment). The overall transfection efficiency at 7 days after gene transfer was ~40%, as assessed by LacZ staining of the LV (Fig. 5*B*). At 7 days after gene transfer, the INH-2 transfected hamsters showed a significant reduction in LV chamber size (LVDd and LVDs; Fig. 5*C* and 5*D*) and an improvement of %FS (Fig. 5*F*) compared with those before the gene transfer, whereas LacZ-treated hamsters showed slight deterioration of %FS and enlargement of LVDd, although these changes in the LacZ group did not reach the level of statistical significance. The index of LV diastolic wall stress, LVDd/PWT, was also significantly attenuated in the AdV-INH-2-treated group compared with the LacZ group (Fig. 5*E*).

INH-2 gene transduction in the CM hamster hearts was confirmed by the immunoblotting for INH-2 (Supplemental Fig. 4*A*). Changes in PP1Cα expression levels and PP1 activities in the cytosol and microsomes were almost identical with those in normal hamsters transfected with the INH-2 gene (an 80% increase in cytosolic PP1Cα and a 30% decrease in microsomal
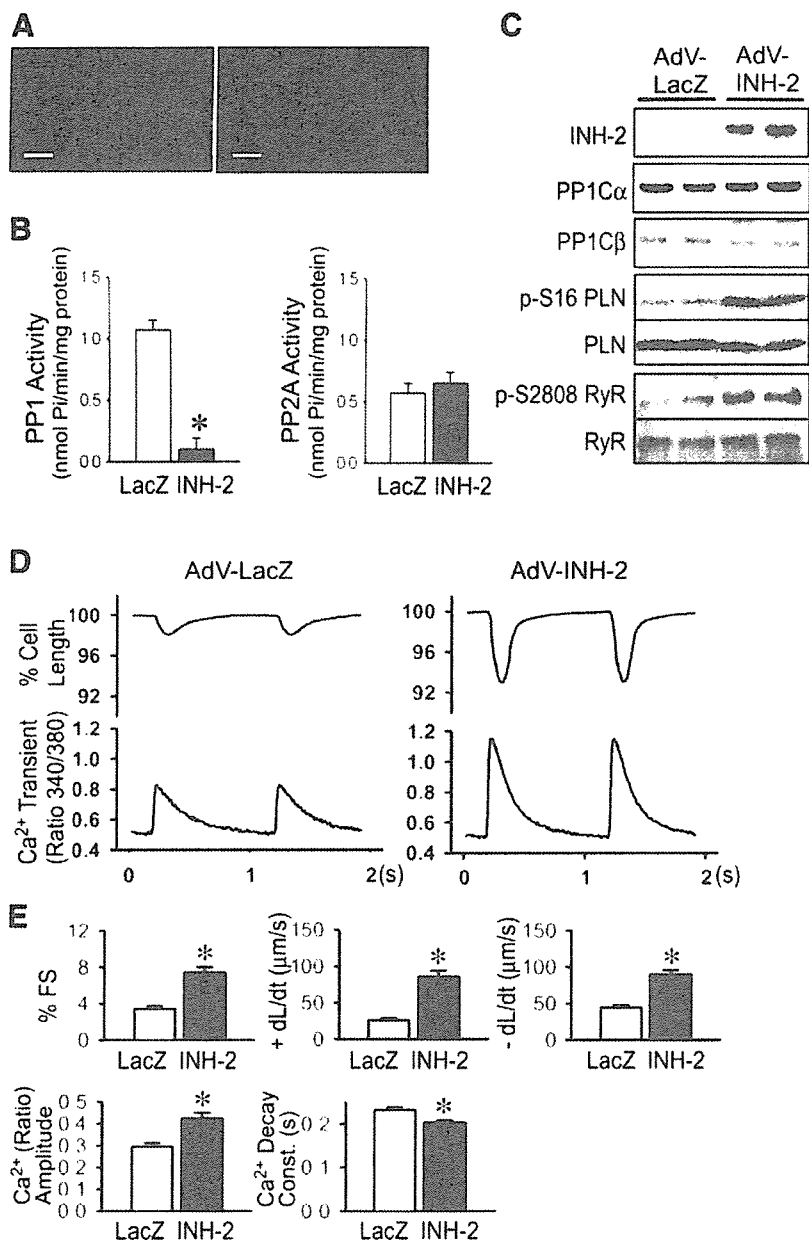
Figure 3. Effect of AdV-INH-2 gene delivery on cell shortening and Ca^{2+} transient in cardiomyocytes. *A)* Immunohistochemical staining of FLAG-tagged INH-2 with anti-FLAG Ab (green) is shown (*left*) together with control staining of wheat-germ agglutinin-conjugated to Alexa633 (red, *right*). The bar indicates 20 μm. *B)* The PP1 and PP2A activities at 36 h after transfection of adenovirus encoding LacZ or INH-2 in adult cardiomyocytes (whole cell homogenate) are shown. *P < 0.05 compared with the LacZ-treated cells (*n*=6). *C)* Representative immunoblots are shown for INH-2, PP1Cα, PP1Cβ, phosphorylated PLN at Ser16 (pS$_{16}$-PLN), total PLN, phosphorylated RyR at Ser2808 (pS$_{2808}$-RyR), and total RyR after *in vitro* adenoviral transfection. *D)* Representative traces are shown for cell shortening and fura-2 fluorescence ratio, an index of the intracellular calcium concentration, after LacZ (*left*), and INH-2 (*right*) gene transfer. (*E*) Indices of contractility are summarized as % FS and +dL/d*t*. The index of relaxation is shown as -dL/d*t*. Indices of calcium transients are shown as the 340/380 ratio of fura-2 fluorescence intensity (Ca^{2+} amplitude). The Ca^{2+} decay time constant (Ca^{2+} decay Const.) of the descending limb of the calcium transients is also shown for AdV-LacZ (open columns), and AdV-INH-2 (solid columns). *P < 0.05 compared with LacZ-treated myocytes.

PP1Cα), except for the slight increase in PP1 activity in the cytosol (Supplemental Fig. 4*C*). Phosphorylation of PLN at Ser16 was increased and that at Thr17 also showed an increasing tendency (**Fig. 6*A***). On the other hand, phosphorylation of RyR at Ser2808 did not show significant change (Fig. 6*A*), and another intracellular PKA phosphorylation target, CREB, did not show any change in phosphorylation at Ser133 by INH-2 gene transfer compared with the LacZ-treated group (Fig. 6*A*). The PKA activity in CM hamster heart at 14 wk was significantly higher than that in normal hamsters. Increased PKA activity in the CM hamster was abnormally higher than that of PKA activity stimulated by intravenous (i.v.) isoproterenol infusion in normal hamsters (Fig. 16*B*). Interestingly, INH-2 gene transfer significantly prevented an abnormal increase in PKA activity, despite the significant increase in PLN phosphorylation at Ser16. Decrease in PKA activity in INH-2-treated hamsters paralleled a decreasing tendency of plasma

catecholamine levels (LacZ vs. INH-2 group: epinephrine, 490±291 vs. 56±21 pg/ml, P = 0.08; norepinephrine, 9862±6001 vs. 4754±1609 pg/ml, P = 0.22; *n*=5 in each group), suggesting that the reduction in the PKA activity was due to the decrease in sympathetic drive. Gene delivery of INH-2 into the CM hamster heart reduced brain natriuretic peptide (BNP) levels (Fig. 6*C*), a predictor of exacerbation of HF, compared with the LacZ-treated group (*P*<0.05, *n*=6 in each group). These results indicate that INH-2 gene transfer has a favorable effect on the failing heart, at least in the short term.

In vivo effect of AAV-INH-2 gene transfer on cardiac function and survival

Because *in vivo* AdV-INH-2 gene delivery resulted in improvement of cardiac function and ameliorated BNP